



Geology and genesis of the Silica-Listwaenite hosted Kaymaz gold deposit, Eskişehir, NW-Turkey: Implications from fluid inclusions and pyrite chemistry

Hikmet Yavuz^a, Yılmaz Demir^{b,*}, Cem Kasapçı^c, İbrahim Uysal^d, Cahit Helvacı^e

^a Koza Gold Corporation, Istanbul Yolu 10. km No: 310, Batkent, Ankara, Turkey

^b Recep Tayyip Erdogan University, Department of Geological Engineering, 53100 Rize, Turkey

^c Istanbul University-Cerrahpaşa, Department of Geological Engineering, 34320 Avcılar, Istanbul, Turkey

^d Karadeniz Technical University, Department of Geological Engineering, 61080 Trabzon, Turkey

^e Dokuz Eylül University, Department of Geological Engineering, 35160 Buca, İzmir, Turkey

ARTICLE INFO

Keywords:

Silica-listwaenite
Kaymaz gold deposit
Fluid inclusion
Mineral chemistry
Northwestern Anatolia

ABSTRACT

The Kaymaz gold deposit comprises Damdamca, Karakaya, Küçük Mermerlik, and Kızılağıl ore zones within an area underlain by serpentinite and far-traveled Paleozoic-Mesozoic high-pressure metamorphic rocks. The Kızılağıl ore zone is hosted in silicified quartz schist, whereas the others are hosted in silica altered serpentinite. Pyrite-I, arsenopyrite, marcasite, magnetite, pentlandite, millerite, nickeline, bravoite, and fine-grained native gold and silver comprise the first stage, whereas pyrite-II and chalcopyrite represent the second ore stage. The Kaymaz gold deposit has been defined as a silica-listwaenite hosted gold deposit according to host rock relations and mineralogical properties.

Gold, Ag, and As were found to be highly correlative in whole-rock silica-listwaenite analyses. Higher As content of the pyrite-I, coexisting native gold and silver together with the whole-rock analyses indicate that these metals were derived from the same source, possibly the Kaymaz granite. On the other hand, clathrate formations observed in some of the first stage fluid inclusions confirm that high Ni in the pyrite-I may have been derived from the serpentinites. However, a distinct lack of the separated carbonic phase and clathrate formations in the second stage fluid inclusions as well as their lower T_h and salinities, reveal that higher Co in the pyrite-II possibly dissolved from the metabasites by meteoric solutions.

1. Introduction

Anatolia hosts many gold deposits, some of which were mined in ancient times, but modern gold mining was limited until the 2000 s. As a result of the increase in gold exploration since the start of the 21st century, a large number of gold deposits have recently been discovered in Turkey (i.e., Bergama, Eşme, Efemçukuru, Kaymaz, and Çöpler). Gold occurrences are particularly concentrated in the west-northwest and northeast parts of Turkey (Fig. 1). The gold deposits in the west-northwest Anatolia mostly formed to the north of the İzmir-Ankara-Erzincan suture zone and are related to Eocene-Early Miocene magmatism, whereas those in the northeast and the eastern Black Sea region are related to the Late Cretaceous eastern Pontide magmatic arc (Yiğit, 2012).

The mining activity in the Kaymaz gold deposit is ongoing. There has

been a production of approximately 900,000 oz of gold in four locations so far, which are called Damdamca, Karakaya, Küçük Mermerlik, and Kızılağıl. Erler and Larson (1990) and Larson and Erler (1992) pointed out that the Kaymaz gold deposit, located between Sivrihisar, Inegöl, and Bursa regions, is one of the most important (e.g., 3 g/t Au) listwaenitic gold mineralization in the region. Yiğit (2006, 2009) proposed that the Kaymaz gold deposit is an orogenic gold deposit that is related to listwaenites. Yavuz et al. (2013) suggested that the Kaymaz deposit is a listwaenite-related epizonal to mesozonal orogenic gold deposit, formed at 240–390 °C from a fluid with salinity ranging from 0.3 to 14 wt% NaCl equ. In this study, the Kaymaz deposit was described as a K-poor metamorphic listwaenite that does not contain fuchsite or mariposite. In contrast, based on quartz $\delta^{18}\text{O}$ and pyrite $\delta^{34}\text{S}$ isotopes (21.5–31.7‰ and –2.6 and –4.7‰, respectively), Toygar (2014) suggested that the ore-forming fluids and sulfur are related to a nearby

* Corresponding author.

E-mail address: yilmaz.demir@erdogan.edu.tr (Y. Demir).

<https://doi.org/10.1016/j.jaesx.2022.100104>

Received 4 March 2022; Received in revised form 11 June 2022; Accepted 14 June 2022

Available online 17 June 2022

2590-0560/© 2022 The Authors. Published by Elsevier Ltd. This is an open access article under the CC BY-NC-ND license (<http://creativecommons.org/licenses/by-nc-nd/4.0/>).

granitic intrusion.

The term "listwaenite" was proposed first time by Rose (1837) for the green rocks from the lode gold deposits of the Miass ore region (South Urals, Russia) (Buckman and Ashley, 2010). Buisson and Leblanc (1985, 1986, 1987), on the other hand, used the term listwaenite to describe an alteration type associated with gold-bearing quartz veins hosted in the ophiolites of northern Italy, western-central Saudi-Arabia, and north-western Africa. However, this term was introduced by Halls and Zhao (1995) to define the rocks formed by low to moderate temperature hydrothermal/metamorphic alteration of mafic-ultramafic rocks within faults or crushed zones. Typically, listwaenites are thought of as a subtype of orogenic gold in which the lode deposits are hosted by mafic-ultramafic rocks and thus have a specific alteration assemblage. Listwaenites may be significant sources of Au, As, Co, Ni, W, and/or Hg elements (Zhelobov, 1979; Kashkai and Allakhverdiev, 1965; Buisson and Leblanc, 1986; Korobeynikov and Goncharenko, 1986; Leblanc and Lbouabi, 1988; Leblanc and Fischer, 1990; Auclair et al., 1993; Sherlock and Logan, 1995; Halls and Zhao, 1995).

The terms "listwaenite" and "silica-carbonate" are synonymous and encompass all forms of carbonatization from the carbonate-rich to silica-rich phases (Buckman and Ashley, 2010). The migration of carbon dioxide-rich fluids along faults causes the modification of serpentinized ultramafic rocks to silica-carbonates, which is referred to as "carbonatization," according to this study. Based on the degree of alteration, silica-carbonates are divided into two categories as phase-1 and phase-2 by Tüysüz and Erler (1993). On the basis of this study, phase 1 silica-carbonates are carbonate-dominated and composed of varying proportions of carbonates, mainly dolomite, ankerite, and rarely siderite, calcite magnesite, and relict serpentinite fragments. On the other hand, carbonate minerals in the phase 2 silica carbonates are either minor or totally absent. Instead, phase-2 silica-carbonates are characterized by the introduction of silica phases such as quartz, chalcedony, and opal. According to Buckman and Ashley (2010), the transition from phase 1 to phase 2 silica-carbonates, SiO₂, CO₂, and K₂O increase in response to volume decreases in MgO and CaO.

Listwaenite occurrences in eastern (Tüysüz and Erler, 1993; Uçurum, 1996, 2000; Çiftçi, 2001) and western Turkey (Aydağ, 1989; Akbulut et al., 2006) were investigated in terms of their alteration assemblage by some researchers, and it was determined that chrome-mica (fuchsite) is absent and that they are also deficient in metals and are typically

uneconomic. However, the origin of the Kaymaz gold deposit is controversial for which the epithermal, listwaenite-hosted orogenic, and intrusion-related models have been proposed. Therefore, the objective of this research was to develop a metallogenic model for the Kaymaz gold deposit. For this purpose, at the first step, geological, mineralogical, and structural properties of each ore veins have been investigated in detail. Whole-rock geochemical analyzes have been performed on the quartz veins and surrounding host-rock samples to clarify the relations between major-trace elements and gold and silver potential of each ore veins. Special attention has been devoted to the fluid inclusion microthermometry and pyrite chemistry of each stage to provide information on the genesis and fluid evolutions processes of the Kaymaz gold deposit.

2. Geological setting

The Kaymaz gold deposit is located in the Tavşanlı zone to the south of the İzmir-Ankara suture zone (Fig. 2a). The Tavşanlı zone represents the high-pressure metamorphic part of the Anatolide-Tauride platform that was overthrust onto the western margin of the Sakarya continent during the Late Cretaceous (Okay et al., 2008). It includes ophiolitic rocks and Ovacık Mélange as well as the exhumed Paleozoic-Mesozoic blueschist facies metamorphic rocks of the Orhaneli Group (Fig. 2b). The Orhaneli Group is composed of, from bottom to top, (i) the Kocasu Formation that consists of quartz-mica schist, (ii) the İnönü Marble that consists of mica schist-marble with chert intercalations, and (iii) the Devlez Formation that consists of metabasite, metachert, and phyllite (Okay, 1986, 2011; Okay et al., 1998). To the east of the Kaymaz deposit, the Sivrihisar Formation crops out, which is composed of marble, metabasite, and mica schist that is commonly altered and in which the high pressure/low temperature (HP/LT) minerals are relatively less preserved (Gautier, 1984; Okay, 2011). This unit corresponds to the Kocasu Formation and İnönü Marble to the west (Okay, 2011). Metabasite, marble, and serpentinites of the Halilbağı Formation crop out to the north of the Kaymaz deposit (Gautier, 1984) (Fig. 2c), which can be correlated with the Devlez Formation (Okay, 2011). The HP/LT minerals in this unit are well preserved (Okay, 2011). Previous studies proposed that the high-pressure metamorphism of the Tavşanlı zone occurred broadly between 175 Ma and 60 Ma (Okay and Kelley, 1994; Harris et al., 1994; Sherlock et al., 1999; Seaton et al., 2009).

Ophiolitic mélangé slices, tectonically overlying blueschists

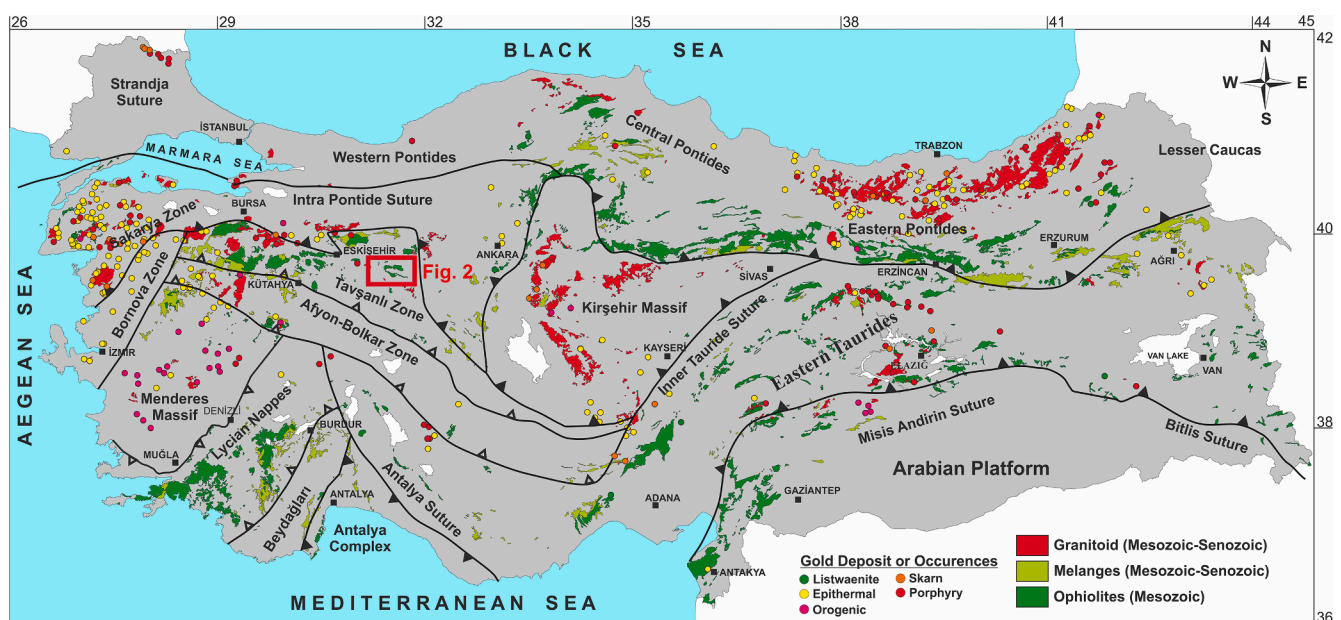


Fig. 1. Locations of gold deposit occurrences and tectonic units of Turkey (MTA, 2002; Robertson and Ustaömer, 2009; Okay and Tüysüz, 1999; Yiğit, 2006, 2009, 2012).

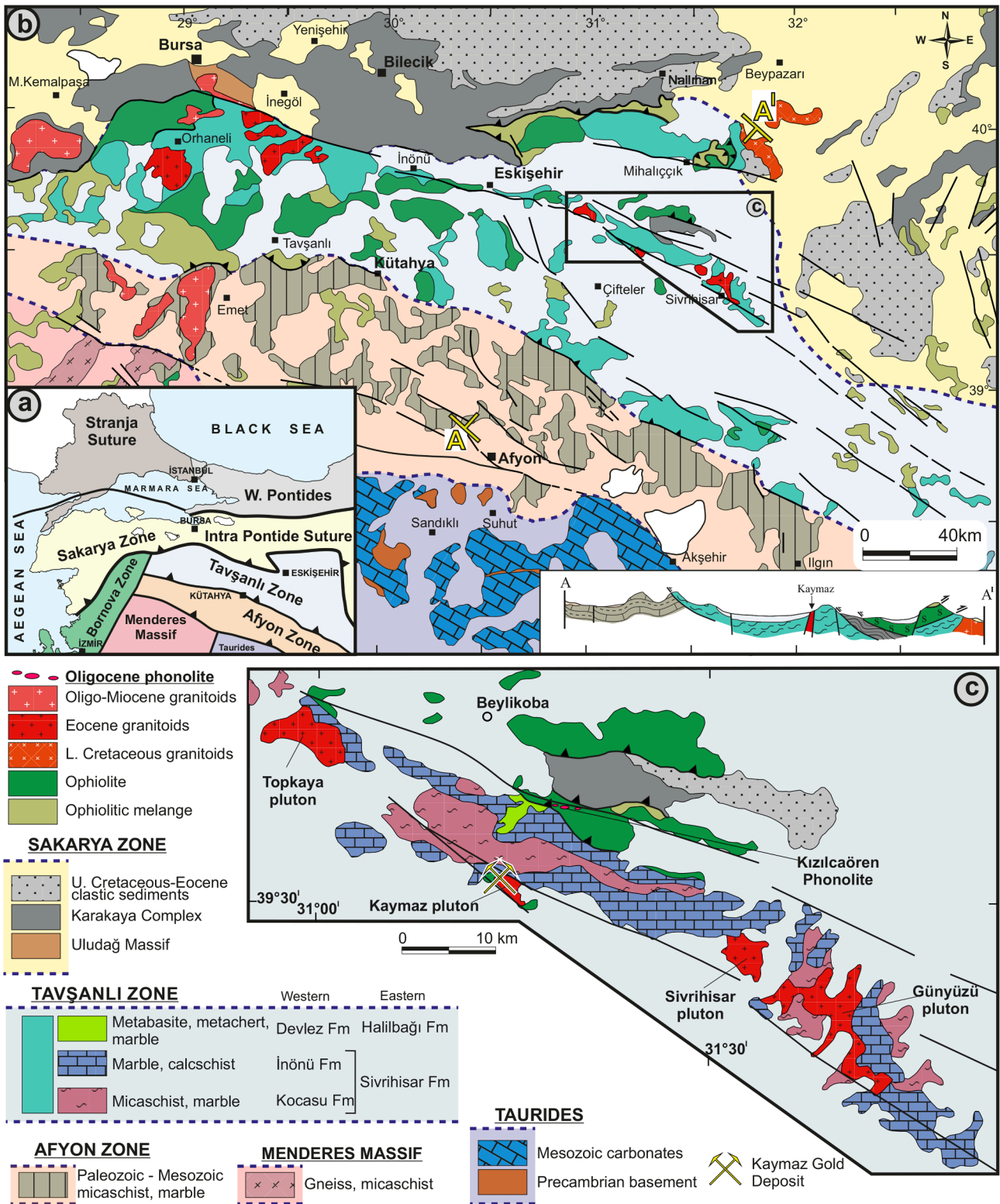


Fig. 2. a) Tectonic map of western Anatolia (modified from Okay and Tüysüz, 1999; Robertson and Ustaömer, 2009), b) Geological map of the Tavşanlı Zone and surrounding area (modified from Okay, 2011; Selçuk and Gökten, 2012), c) Geologic map showing the major units of the Kaymaz and surrounding area (modified from Gautier, 1984; Selçuk and Gökten, 2012).

belonging to the Tavşanlı zone, are known as the Ovacık Complex (Kaya, 1972). This unit is composed of basalt, radiolarian chert, pelagic shale, limestone, and lesser serpentinite, greywacke, and layered manganese (Okay, 2011). Radiolarian ages obtained from these units range from Late Triassic (late Carnian-late Norian) to Late Cretaceous (Cenomanian-

Turonian) (Tekin et al., 2002; Göncüoğlu et al., 2006).

Late Cretaceous to Eocene plutons intrude into the WNW-ESE trending Tavşanlı Zone that is exposed from the Kapıdağ Peninsula in the northwest to the Sivrihisar in the southeast (Okay and Whitney, 2010; Altunkaynak et al., 2012; Shin et al., 2013). Isotopic ages from

Table 1
Some reported intrusion ages of the granitoids from the Tavşanlı Zone of northwestern Anatolia.

Tectonic Zone	Granitoid	Method	Mineral	Age (Ma)	References
Afyon Zone	Şamlı	Ar–Ar	Biotite	22.3 ± 0.1/21.9 ± 0.1	Altunkaynak et al., 2012
	Çataldağ	U–Pb	Zircon	21.9 ± 0.3	Altunkaynak et al., 2012
	Eğrigöz	U–Pb	Zircon	19.5 ± 0.3	Altunkaynak et al., 2012
Tavşanlı Zone	Orhaneli	U–Pb	Zircon	52.8 ± 1.87	Altunkaynak et al., 2012
	Topuk	U–Pb	Zircon	48.71 ± 0.44	Altunkaynak et al., 2012
	Tepeldağ	U–Pb	Zircon	44.99 ± 0.23	
		U–Pb	Zircon	45.41 ± 0.34	Altunkaynak et al., 2012
	Gürgenyayla	U–Pb	Zircon	51.02 ± 0.52	Altunkaynak et al., 2012
	Sivrihisar	U–Pb	Zircon	90.82 ± 2.14	Gautier, 1984
		U–Pb	Zircon	42.4 ± 2.3/78.4 ± 8.5	Shin et al., 2013
	Kaymaz	U–Pb	Zircon	84.98 ± 6.27	Gautier, 1984
		U–Pb	Zircon	33.3 ± 2.0/42.5 ± 2.2	Shin et al., 2013
		U–Pb	Zircon	65.91 ± 3.84	Gautier, 1984
Sakarya Zone	Yörükkaracaören	U–Pb	Zircon	66.93 ± 4.86	Gautier, 1984
	Beypazarı	U–Pb	Zircon	72.5 ± 12.6/78.6 ± 4.7	
	Uludağ metagranite	U–Pb	Zircon	34.71 ± 0.34	
	Uludağ Granite	U–Pb	Zircon	28.24 ± 0.39	

these plutons range widely from 90.8 ± 2.1 to 34.3 ± 0.9 Ma (Table 1). Deleloye and Bingöl (2000) indicated that mineralogical and geochemical compositions of these granitoids range from calc-alkaline granites to granodiorites and monzogranites to syenogranites. According to Şahin et al. (2006) and Shin et al. (2013) the SiO₂ content of the Kaymaz and Sivrihisar granites, which has a sub-alkaline composition, is higher than other igneous rocks in this zone. Furthermore, alkaline volcanic rocks (phonolite) and carbonatites, dated at 24 Ma, are located ~ 14 km north of the Kaymaz deposit (Sarrafakıoğlu et al., 2009; Niki-forov et al., 2014) (Fig. 2c). Rocks of the Pliocene to Pleistocene İlicabaşı Formation, which consist of conglomerate, sandstone, mudstone, claystone, marl, limestone, gypsum and peat, unconformably overlie all the above units (Saraç, 2003; Selçuk and Gökten, 2012).

3. Analytical techniques

Bulk rock geochemical analyses of 98 ore vein samples were determined for their major and trace element concentrations at the ACME Analytical Laboratories Ltd., Vancouver (Canada) using total digestion Inductively Coupled Plasma-Emission Spectroscopy (ICP-ES). All geochemical data were provided by the Koza Gold Company and are only presented here in summary. The analytical precision of the method for each element is within the limits expected for research quality analyses. Detection limits range from 0.01 to 0.1 wt% for major oxides and from 0.1 to 10 ppm for the trace elements.

The compositions of ore minerals were analyzed from representative samples selected from each location using a Cameca SX-100 wavelength-dispersive electron probe micro-analyzer (EPMA) at the Department of Earth and Environmental Sciences of the Ludwig Maximilian University in Munich, Germany. The operating conditions were 15–20 kV accelerating voltage, 20nA beam current, and counting times of 20 s per element. Calibrations were performed using pure elements and minerals as standards. The L α X-ray lines were measured for As, Ag, Sb, and Cd, the K α lines were measured for S, Cu, Fe, and Zn, and the M α lines were measured for Pb. The limits of detection for each element were calculated using the 3 σ statistical precision approach and are given in parenthesis (in ppm): Fe (500), Zn, As, Sb (800), Ag (1000), Cu, Ni, Co (600), S (300), Hg, Au (400).

Microthermometric measurements of fluid inclusions were carried out using a Leica DMLP polarized microscope mounted Linkam THMG-600 heating–cooling system (-196 °C and 600 °C) in Istanbul University-Cerrahpaşa, Department of Geological Engineering. Homogenization temperature (T_h), eutectic temperature (T_e), final ice melting (T_{m-ice}), and clathrate melting temperature (T_{m-clth}) of fluid inclusions were measured using wafers approximately 200 μ m in thickness and double-side polished. Before the measurements, the device was calibrated using

synthetic fluid inclusions. Repeated measurements have shown accuracies of ± 3 °C for positive values and ± 0.2 °C for negative values. The salinities of liquid–vapor type (LV) aqueous inclusions have been calculated based on the equilibrium proposed by Roedder (1984) using the T_{m-ice} . The salinities of inclusions with detected clathrate have been calculated according to Darling (1991) using T_{m-clth} . Possible salt compositions of the fluid were interpreted according to Shepherd et al. (1985), taking into account the T_e of the fluid inclusions.

4. Results

4.1. Geology of the Kaymaz gold deposit

The basement units of the Kaymaz area are represented by quartz schist, calcschist, and marble of the Sivrihisar Formation (Fig. 3). Quartz schists are observed as N-S trending discrete bodies (Fig. 3) and are highly brecciated in the Kızılağıl zone. The silicification filling between these breccias occasionally shows zoned growth towards the cavities (Fig. 4a). The calcschists in the deposit area crop out along a well-defined NW-striking-trend (Fig. 3). In the vicinity of the Karakaya village, they show foliation structure, and chlorite, epidote, and amphibole are commonly found in the calcschists (Fig. 4b). Brecciation and silicification are common along with the contact between calcschists and serpentinites, and yellowish-brown colors characterize such altered rocks due to oxidation of Fe-oxide minerals. The marbles are commonly banded and show granular texture. However, in some cases, they are brecciated (Fig. 4c) and are widely cut by discontinuous quartz veins. In the vicinity of the Kızılağıl and Küçük Mermerlik ore veins, the marbles are unconformably overlain by the Neogene sediments.

Serpentinites are the host rock of the Kaymaz gold deposit; they crop out to the west and southeast of the Kaymaz granite and are commonly silica-altered (Fig. 4d). The rocks are intensely oxidized and surround the ore zones. On the west side of the Damdamca ore zone, the serpentinites tectonically overlie the marbles. Alteration and brecciation decrease away from the tectonic contact, while the foliation-related structures become more apparent along with the contact. Chalcedony and magnesite occur along with fractures in the serpentinites that also host the auriferous quartz veins (Fig. 4e).

The Eocene Kaymaz granite intrudes into these units (Fig. 3) and is composed of quartz, K-feldspar, plagioclase, and biotite and includes mafic enclaves. In the vicinity of the Damdamca ore zone, serpentinite is locally cut by granite, and both were subsequently affected by hydrothermal alteration. A thick zone of silicification with iron oxide is observed along with the contact between the granite and serpentinites (Fig. 4f).

A younger NW-trending dextral fault zone separates the contact

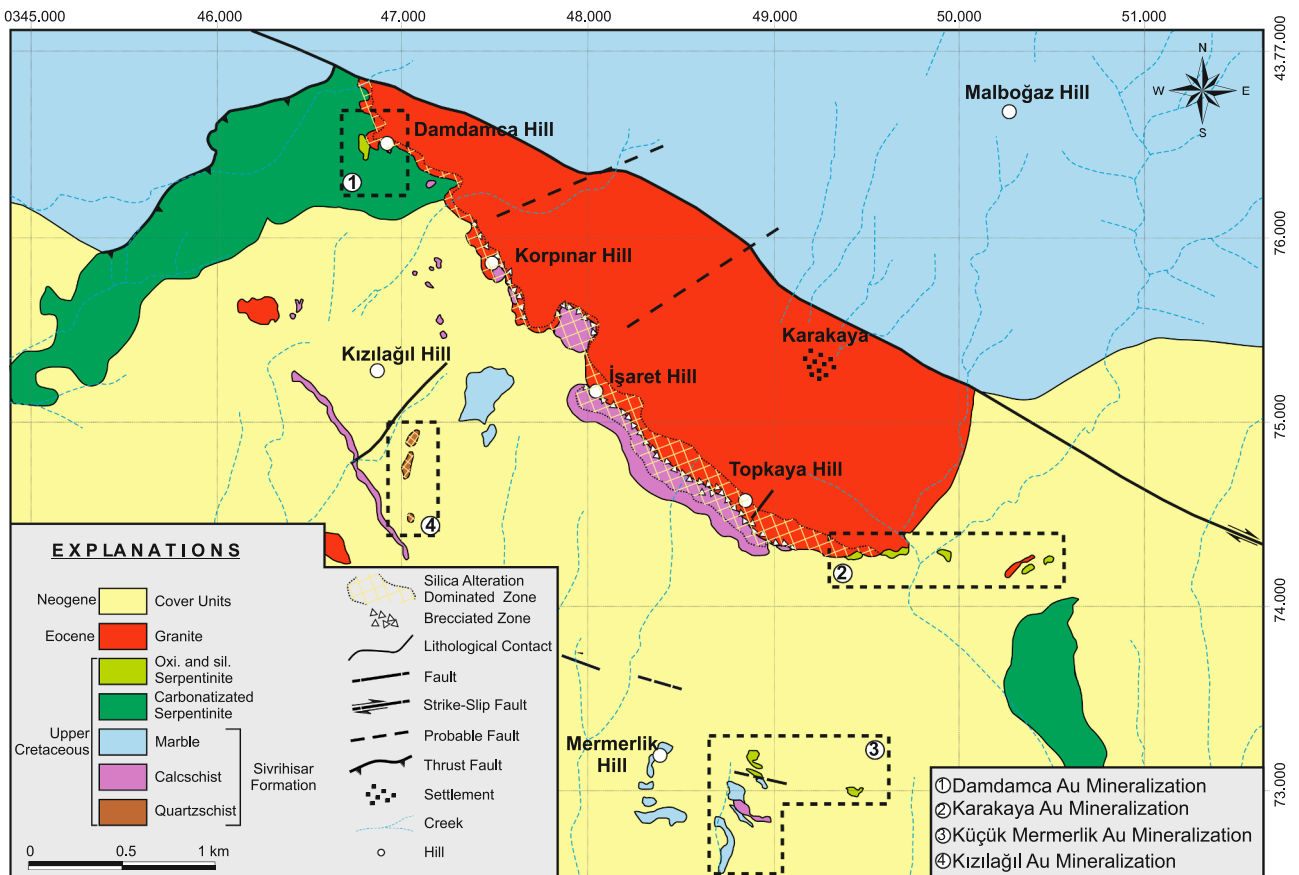


Fig. 3. Geology map of the Kaymaz gold deposit and surrounding area (Yavuz, 2013).

between the Kaymaz granite and Tavşanlı marbles. Contact metamorphism or metasomatic features are absent at the northern contact of the granite with the marbles because a younger fault zone characterizes this contact. However, along with the southern contact, brecciation and argillic alteration are common (Fig. 4f). Sericitization, chloritization, and epidotization have also been observed in the granite. Silicification has affected the granite, as evidenced by cross-cutting quartz veins. Stockwork quartz veins are also common in close proximity to the main quartz veins. The general features of the Damdamca, Karakaya, Kızılağıl, and Küçük Mermerlik ore zones were described below.

4.1.1. Damdamca ore zone

The Damdamca ore zone is located along the intensively silicified serpentinite-granite contact, which is partly covered by the Neogene sedimentary rocks. The serpentinite-granite contact was terminated through the SE direction, and a new contact between calcschist and granite was developed due to this fault zone. A distinct lack of skarnization along the calcschist and younger granite contact confirms subsequent fault development. The granite underwent argillic alteration, and silicification is locally seen in the calcschists.

The Ore zone in the area lies approximately 250 m south of the strike-slip fault zone between marble and granite, and parallel to this fault zone with a NW trending and 60° dips to the NE direction (Fig. 3). Ore-bearing veins reaching up to 2 m in thickness (Fig. 5a) are commonly dominated by massive and vuggy quartz (Fig. 5b). These quartz veins are always surrounded by the stockwork and disseminated ore textures (Fig. 5c) in the host rocks which reflect infiltration of the hydrothermal solutions. Minor calcite and barite were formed through the end of the first stage of gold-bearing quartz veins. The second hydrothermal stage, on the other hand, was characterized by pyrite- and chalcopyrite-bearing quartz veins, which cross-cut the stockwork ore

zone (Fig. 5d). The average gold content is approximately 6.0 g/t in the Damdamca ore zone.

4.1.2. Karakaya ore zone

The Karakaya ore zone formed in silicified serpentinite along with the contact between the Kaymaz granite and oxidized serpentinite (Fig. 3). The dip of the ore zone, which is discontinuously exposed in an E-W direction of approximately 1.5 km, is 65° to the south. The silicified rocks can be followed from an area east of Topkaya Hill to Damdamca Hill. Silicification also occurs along with the contact between calcschist and granite in the İşaret and Korpınar hills, but the gold grade is very low in that area (Fig. 3).

The first stage ore minerals in the silicified serpentinites were characterized by fine- to coarse-grained quartz veins. Fine-grained quartz veins mostly show a vuggy texture. In addition, these quartz veins become narrow argillic alteration zones and silicification haloes in granite (Fig. 5e). First stage quartz veins were surrounded by the stockwork (Fig. 4e) and disseminated ore textures in the serpentinites. It has been observed that second stage quartz veins with a few centimeters in width and a few meters in length cut stockwork and disseminated ore zone (Fig. 5f). Late-stage chalcedony (Fig. 5g) and magnesite (Fig. 5h) veins are observed as supergene features in serpentinite and granite. The Karakaya ore zone has an average Au content of 4.0 g/t.

4.1.3. Küçük Mermerlik ore zone

The Küçük Mermerlik ore zone is located roughly 1.5 km south of the Kaymaz granite. The ore zone is discontinuously exposed in places where Neogene cover units are absent. The ore zone comprises a zone of brecciation along with the contact between the serpentinite and marble. The breccia zone, with a dip of 50° to the north, consists of silicified serpentinite, marble, and quartzite breccias. Two different stages of ore

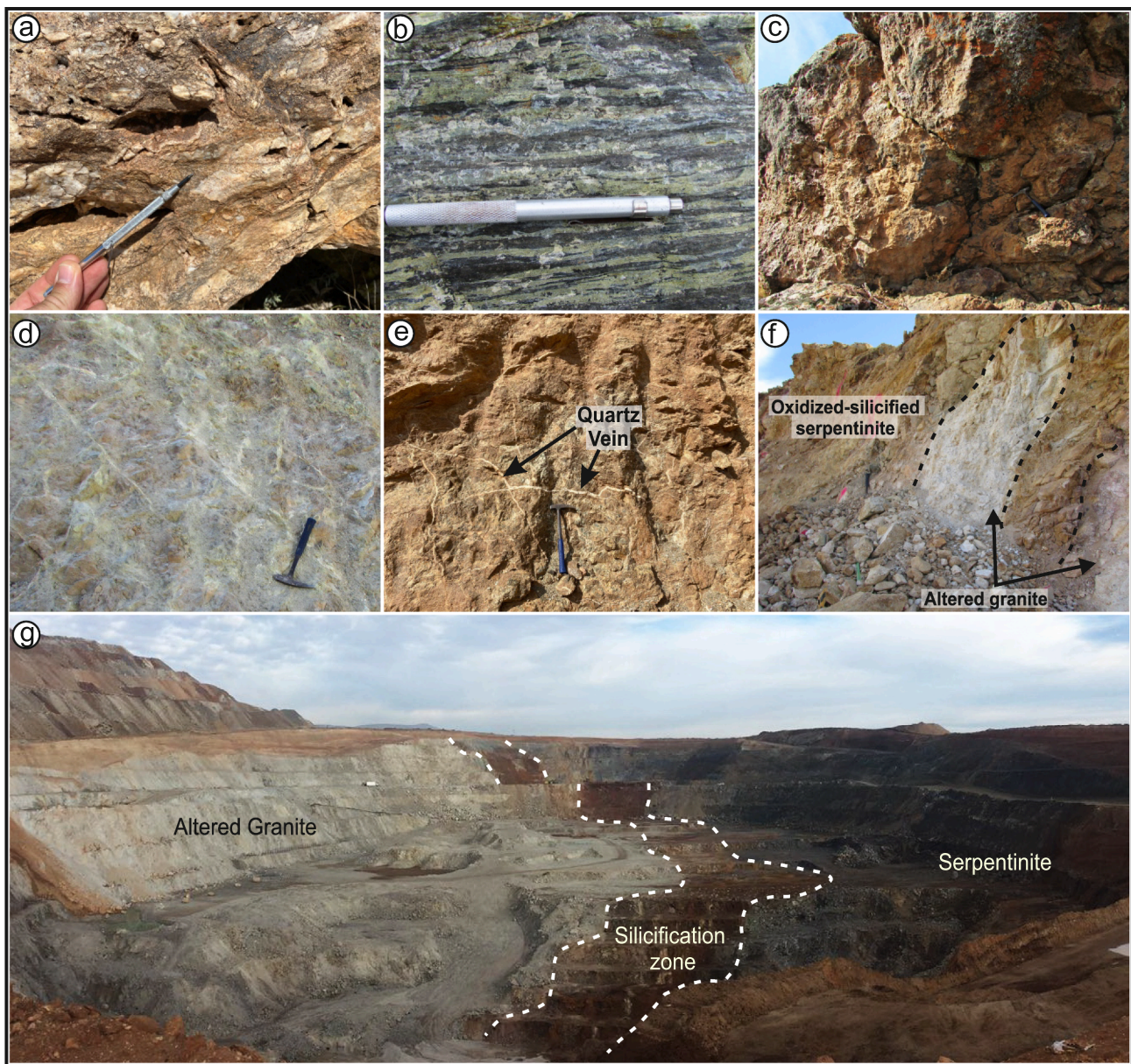


Fig. 4. a) Growth zonation towards the cavities in the brecciated quartz schist in the Kızılağıl ore zone, b) Foliation structure of the calcschist in the Karakaya village, c) Brecciation structure in the marble, d) Silica-altered serpentinite, e) Quartz veins, a few meters long, cutting the serpentinite, f) Silicified and oxidized serpentinites cut by argillically altered granite, g) General view of the alteration zone between serpentinites and Kaymaz granite.

minerals were described in the Küçük Mermerlik area. The first stage was represented by silicified serpentinite, marble, and breccia fillings textures in the quartz schist (Fig. 5i). The second stage, on the other hand, was represented by minor quartz veins cutting the host serpentinites (Fig. 5j). Calcite pseudomorphs and black quartz-chalcedony were found to be filling the gaps as a product of the supergene stage. The average Au content of the ore zone is approximately 2.0 g/t.

4.1.4. Kızılağıl ore zone

The Kızılağıl ore zone is located in quartz schist. Silicified quartz schist is discontinuously exposed along a 400 m long, N-S trending zone. The early quartz veins and silicified quartz schist represent the first stage of ore minerals in the Kızılağıl ore zone. Cockade and comb textured quartz accompany vuggy-textured quartz crystals in this early stage ore minerals (Fig. 5k). The silicified quartz schist and early quartz veins, which are mostly yellowish-brown due to supergene oxidation were observed to be highly brecciated. As a result of the supergene stage,

calcite pseudomorphs and black quartz-chalcedony were seen to be filling the gaps. (Fig. 5l). The average content of gold is approximately 3.0 g/t.

4.2. Ore mineralogy

Two different stages of ore were macroscopically described in the Kaymaz gold deposit. The first stage was observed as quartz veins throughout the host serpentinite, granite, and quartz schist. These ore veins are always surrounded by the stockwork and disseminated ore minerals throughout the main ore veins, which refer to the infiltration of ore-bearing hydrothermal solutions at the first stage of ore minerals. In the microscopic investigations, the Kaymaz area is represented by highly fractured chromium spinel grains due to tectonic deformation in the region (Fig. 6a). These chromium spinel grains are mostly altered to magnetite prior to the gold-related hydrothermal event. The first stage ore minerals were described along the fractures of these chromium

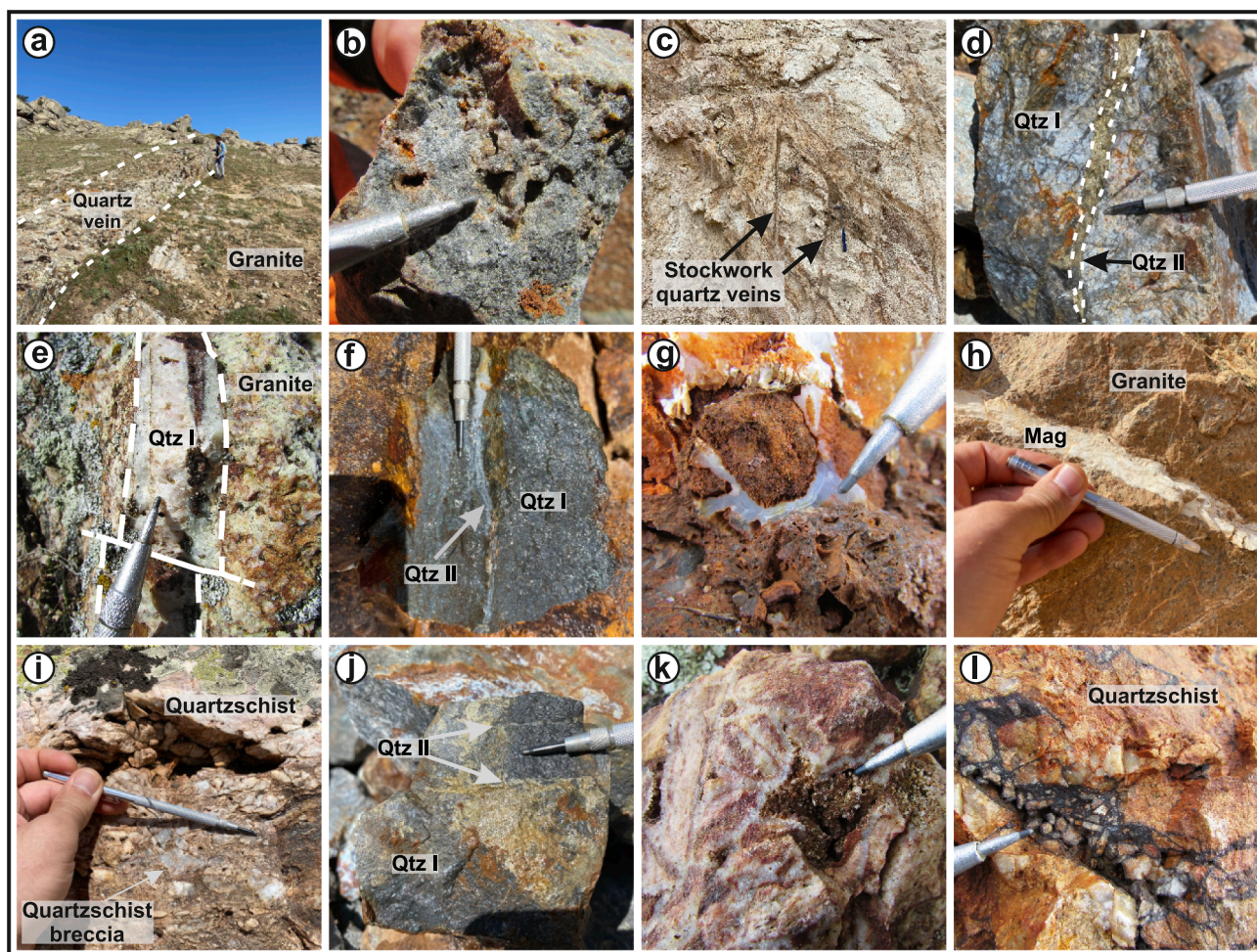


Fig. 5. a) Gold-bearing quartz vein in the Kaymaz granite, b) Vuggy quartz in the Damdamca ore zone, c) Stockwork quartz veins around the main quartz vein in the Kaymaz gold deposit, d) Second stage quartz vein in the first stage ore vein, e) Argillic alteration and silicification along the minor quartz veins in granite, f) Disseminated first stage mineralization in serpentinites and second stage quartz vein, g) Chalcedony development in supergene stage, h) Magnesite veins in the granite, i) Breccia filling texture in the quartz schist, j) Second stage quartz veins cutting the serpentinites, k) Cockade texture of the early stage quartz in the Kızılağil ore zone, l) Breccia filling second stage mineralization in the Kızılağil ore zone.

spinel and magnetite grains and mostly include pyrite-I, bravoite, marcasite, and chalcopryite (Fig. 6a). In some cases, pyrite-I and bravoite are observed to envelop the chromium spinel and magnetite (Fig. 6b). The first stage pyrite-I is also observed as fine to medium-grained pseudomorphs. In some cases, coarse-grained euhedral crystals were also observed (Fig. 6b). Boundaries between the pyrite-I and marcasite are irregular in shape (Fig. 6c). Pyrite-I and bravoite intergrown indicate a coeval formation (Fig. 6d). Millerite, pentlandite, arsenopyrite, and nickeline were found in ore veins in this stage and accompanied pyrite-I, bravoite, and marcasite (Fig. 6e). Arsenopyrite is present as euhedral-subhedral single crystals in the gangue (Fig. 6f). In the quartz-I gangue, native gold and silver, which are smaller than 5 μm , are mostly observed as separate grains (Fig. 6g, h), and sometimes they are associated (Fig. 6i). This gold and silver-bearing quartz-I predate the second phase because second stage quartz veins were found to be cutting first stage (Fig. 6j).

Pyrite dominated, and rarely chalcopryite-bearing quartz veins cutting the first stage stockwork and disseminated ore were described macroscopically as a second stage ore minerals in the Kaymaz area (Fig. 5d, f, j). By the microscopic investigations, pyrite-II is observed as pseudomorphs, which are smaller, subhedral/euhedral, and more disseminated compared to the pyrite-I grains (Fig. 6j). Pyrite-II is found as pseudohexagonal crystals in all four ore zones. A limited amount of chalcopryite inclusions coexisting with pyrite-II were determined in the

second stage quartz veins of the Karakaya ore zone (Fig. 6k). Replacement of chalcopryite by chalcocite/covellite is limited. Hematite, goethite, limonite, chalcocite, covellite, lepidocrocite, and pyrolusite were formed in the supergene stage of the Kaymaz deposit. Pyrite-I and Pyrite-II were transformed into goethite and limonite, whereas magnetite was altered to hematite (Fig. 6-l). The mineral paragenesis and succession of the Kaymaz gold deposit were produced as a consequence of the macroscopic and microscopic studies discussed above, as illustrated in Fig. 7.

4.3. Mineral chemistry

In this study, special attention was devoted to the pyrite chemistry since gold in the Kaymaz deposit accompanies pyrite minerals and the composition of these minerals gives significant information in determining the source of hydrothermal solutions. Two different types of pyrites (pyrite-I and pyrite-II) were identified in the petrographic studies, and the results of the mineral chemistry analysis from both types are given in Table 3. Pyrite-I is always characterized by Au content of up to 0.1 wt%, while the Au content of pyrite-II, in all measurements, is below the detection limit. Au-bearing pyrite-I is represented by higher As contents ranging between 0.1 and 8.0 wt%. Arsenic in pyrite-I has a limited negative correlation with Fe (Fig. 8a) but a high negative correlation with S (Fig. 8b) due to the arsenic sulfur incompatibility.

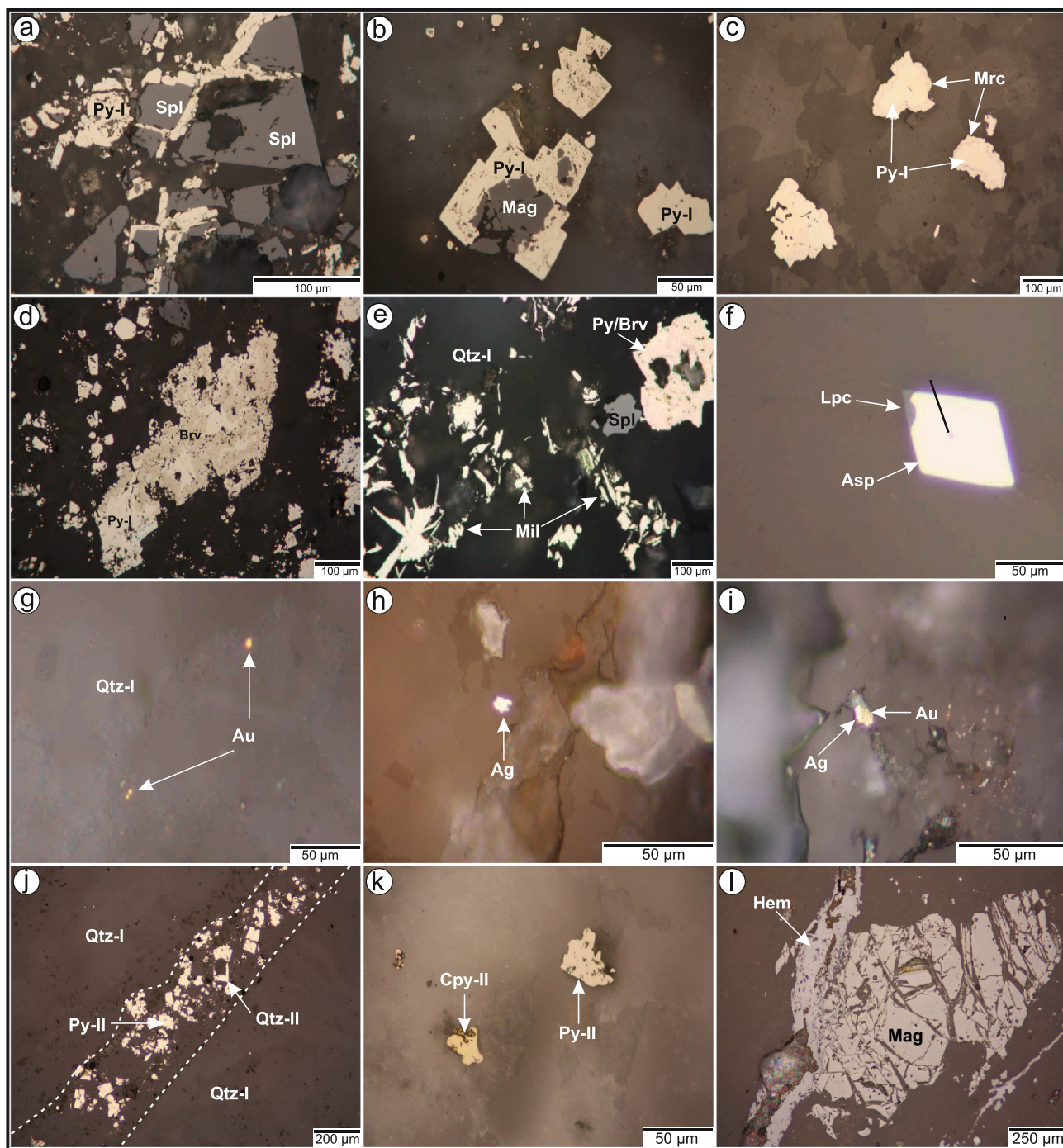


Fig. 6. a) Highly fractured spinel grains and fracture filling mineralization of early stage pyrite, b) Euhedral pyrite-I overgrowth on the magnetite crystal, c) Marcasite overgrowth on the pyrite-I pseudomorphs, d) Pyrite-I and Bravoite intergrown at the first ore stage, e) Pyrite-I and bravoite presenting growth zoned, radial and euhedral millerite minerals within the gangue, f) Lepidocrocite replacement at the edge of euhedral arsenopyrite mineral, g) Native gold crystals observed in quartz-I, h) Ag crystal observed in quartz-I, i) Gold and silver alloy in the first stage quartz-I, j) Second stage quartz-II vein in the early stage quartz-I, and pyrite-II dissemination along the quartz vein, k) Coeval pyrite-II and chalcopyrite-II minerals in the second stage quartz-II, l) Hematite replacement of the magnetite through the fracture.

Arsenic in these pyrite-I positively correlated with Au (Fig. 8c). Up to 1 wt% Hg was measured from pyrite-I, whereas Hg values of the pyrite-II were lower than 0.1 wt%. Au-bearing pyrite-I is always characterized by higher As and Hg contents, whereas these values are close to the detection limit in the Au-free pyrite-II (Fig. 8d). The Ni contents of these high As-bearing pyrite grains are also high, and range between 0.1 and 0.9 wt% (Fig. 8e), whereas the Ni contents of pyrite-II are lower than 0.6 wt%. While the Co content of pyrite-I is below the detection limit in all

measurements, the Co content of pyrite-II is generally higher (reaching up to 3.49 wt%), and the values correlate with Fe (Fig. 8f).

4.4. Trace element geochemistry

Whole-rock samples taken from drill cores and surface veins in the Kaymaz deposit have been analyzed for selected elements. The maximum Au content of 78.3 ppm is from the Karakaya ore zone,

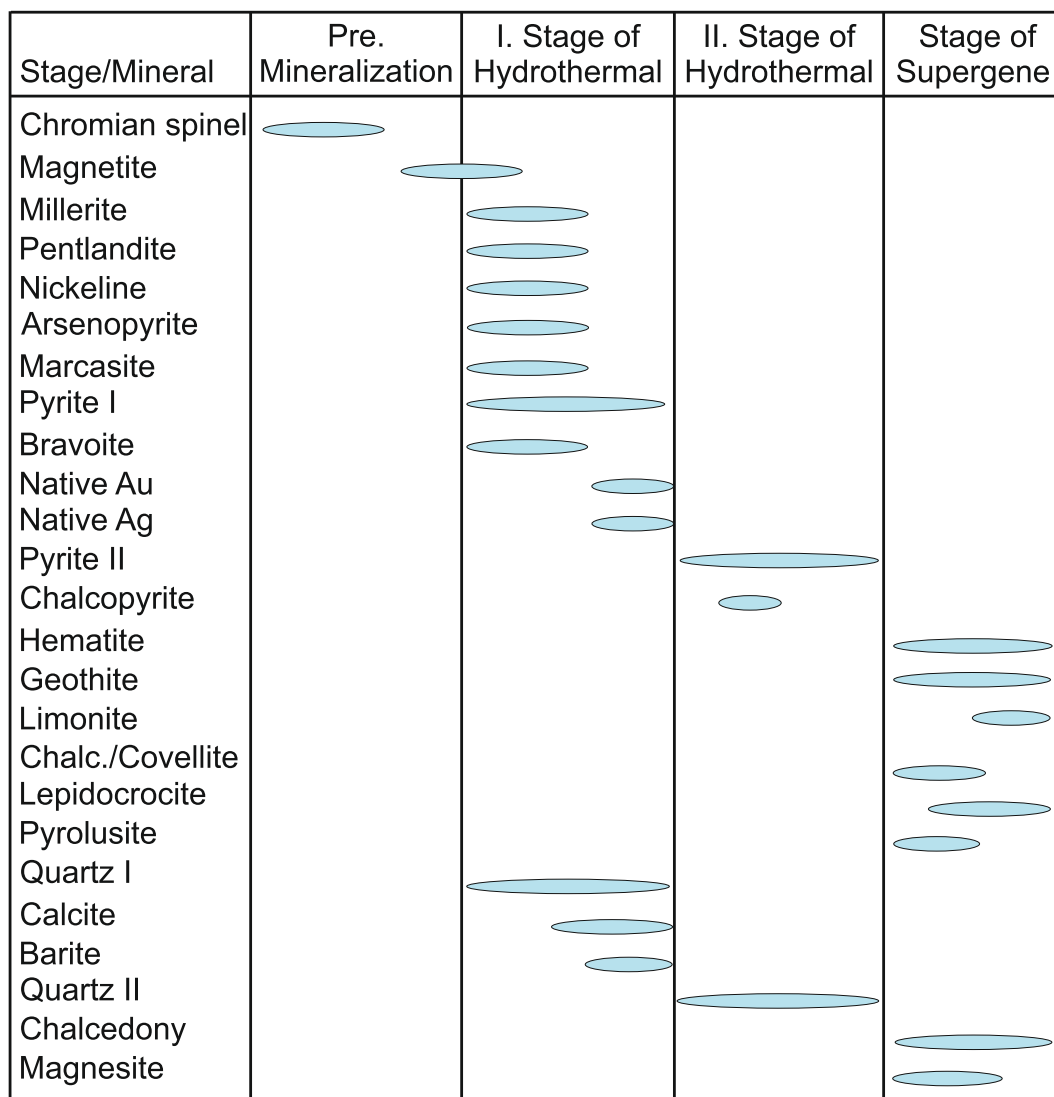


Fig. 7. The paragenetic sequence of the Kaymaz gold deposit (Modified after Yavuz et al., 2013).

whereas the maximum Ag content of 69.3 ppm is from the Kızılağıl ore zone. Besides, the mineralized samples contain as much as 408 ppm Co, 9950 ppm Ni, 145 ppm Cu, 9433 ppm Zn, and 1645 ppm Pb (Table 2). Arsenic (As) and Cr contents in some samples exceed 1 wt%. The average Au and Ag content of 88 samples are 5.87 and 6.12 ppm, respectively (Table 2). The Damdamca and Karakaya ore zones, which contain the highest part of the resource in the Kaymaz deposit, contain averages of 10.43 ppm ($n = 21$) and 8.50 ppm ($n = 23$) Au, respectively, whereas these locations contain averages of 9.15 ppm and 9.38 ppm Ag. For the Küçük Mermerlik ($n = 21$), and Kızılağıl ($n = 23$) mineralized zones averages Au contents are 2.47 and 2.17 ppm, and Ag contents are 2.19 and 3.33 ppm, respectively.

The Au and Ag concentrations are strongly positively correlated (Fig. 9a), whereas Au shows weak positive correlations with As, Hg, and S (Fig. 9b, c, d). Au has a positive correlation with Co and Ni in the Damdamca and Karakaya samples, whereas no relation was observed in the Kızılağıl and the Küçük Mermerlik samples (Fig. 9e, f). Besides, when all of the results are evaluated together, positive correlations appear between element pairs of Ni-Co, As-Ni, and As-Co (Fig. 9g, h, i). The average Ni/Co ratio is 21, with individual samples ranging from 6 to 43.

4.5. Fluid inclusions

4.5.1. Petrography of the fluid inclusions

Petrographical properties of the fluid inclusions in each sample were defined before freezing and heating experiments. Primary and secondary inclusions were classified using the criteria described by Roedder (1984) and Van den Kerkhof and Hein (2001) in doubly polished sections. In this study, only primary inclusions were measured because secondary inclusions were probably affected by processes following ore formation. In addition to two-phase liquid-vapor (L + V) fluid inclusions (Fig. 10a, b), monophasic fluid inclusions are also present in the investigated sections. However, microthermometric measurements were performed only on two-phase inclusions since phase transitions could not be observed in single-phase inclusions. There were no halite- or CO₂- bearing fluid inclusions visible at room temperature.

According to the petrographic studies, the first stage quartz is cut by the second stage quartz, or the second stage quartz fills in the fractures of the early stage quartz breccias. Quartz from both stages was found to contain mostly irregular fluid inclusions. Besides, less abundant circular, elliptical, and tube-shaped inclusions were also observed (Fig. 10c). Fluid inclusions in both stages of quartz vary widely in size from a few to 30 μm . The degree of fill of the liquid-rich fluid inclusions in the first stage quartz range from 0.8 to 0.5 (Fig. 10b), whereas, lower liquid

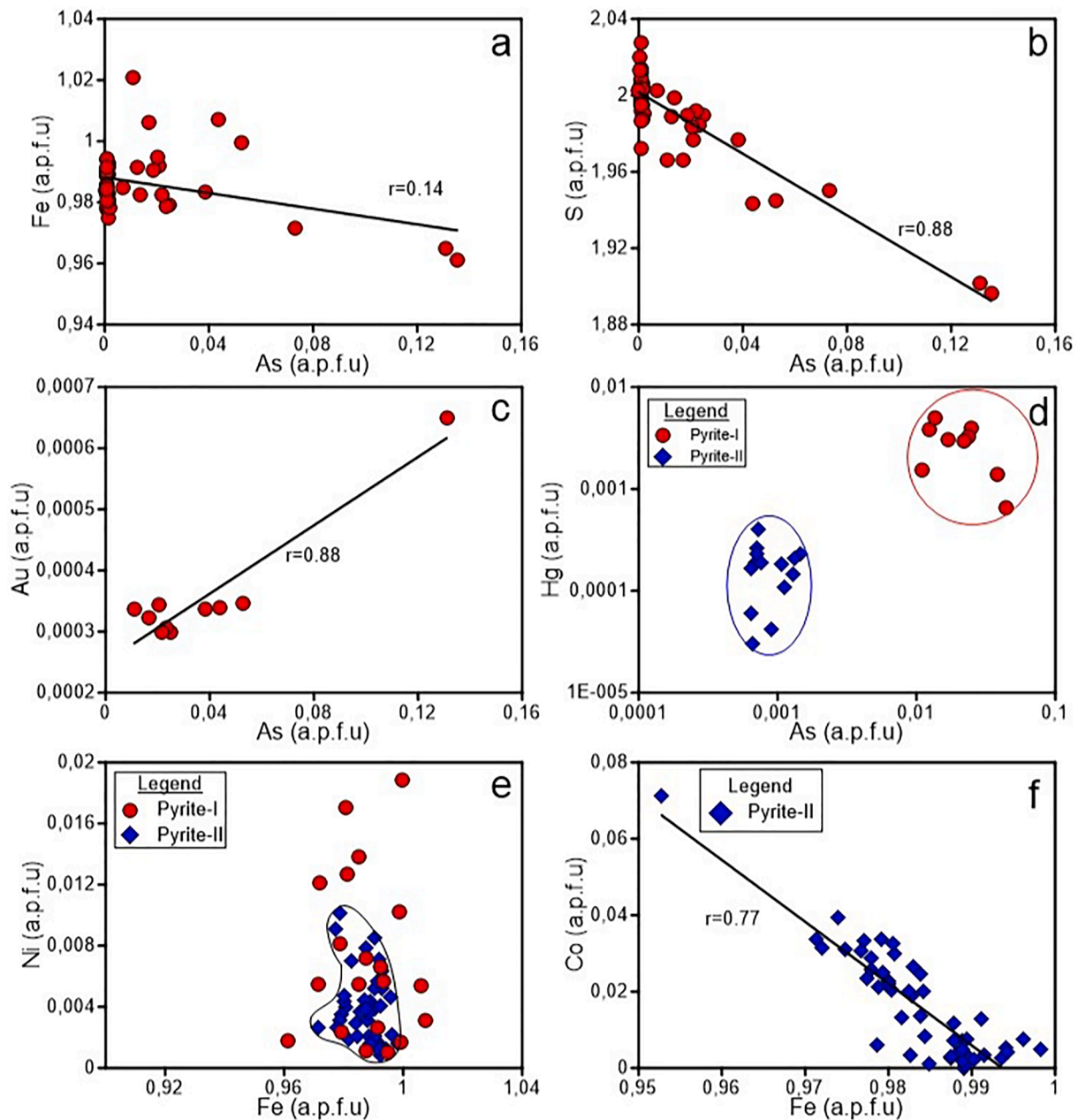


Fig. 8. Major and trace element concentrations of pyrites from the Kaymaz listwaenite and some correlative relationship between the elements Fe, As, S, Ni, Co, Au, and Hg.

ratios were observed in coexisting vapor-rich fluid inclusions (Fig. 10b, d). It has been observed that while liquid-rich fluid inclusions were always homogenized to the liquid phase, some of the vapor-rich fluid inclusions were homogenized to vapor phases. Although there are no characteristic differences between the two stages regarding inclusion shape, size, and phase numbers at room temperature, the second stage fluid inclusions were found to have lower vapor ratios (0.1–0.3), and all these inclusions homogenized to liquid phases.

4.5.2. Microthermometric results of the fluid inclusions

The homogenization temperatures (T_h) of the first stage fluid inclusions in quartz have been measured from the Kızılağıl location, while both stage fluid inclusions have been measured from the quartz minerals of the Küçük Mermerlik, and Karakaya locations of the Kaymaz gold deposit. The T_h values measured in the first stage samples from the Kızılağıl area vary between 279 and 382 °C with an average of 340.5 °C

($n = 25$). In the Küçük Mermerlik, and Karakaya locations, T_h values of the first stage fluid inclusions are in the range of 328–389 °C (average 339 °C, $n = 22$), and 316–374 °C (average 347 °C, $n = 26$), respectively (Table 4, Fig. 11a). On the other hand, T_h of the second stage fluid inclusions was measured between 238 and 268 °C (average of 252 °C, $n = 7$) in the Küçük Mermerlik, and between 237 and 298 °C (average of 267 °C, $n = 25$) in the Karakaya locations.

Final ice melting temperatures (T_{m-ice}) of both stages of fluid inclusions from the Küçük Mermerlik and Karakaya ore veins, and first stage fluid inclusions from the Kızılağıl location were measured to determine the salinities of the hydrothermal solutions. T_{m-ice} temperatures of the first stage fluid inclusions were measured in the range of –0.6 to –7.3, –0.1 to –1.5, and –0.4 to –11.4 °C in the Küçük Mermerlik, Kızılağıl, and Karakaya locations, respectively (Table 4). The T_{m-ice} temperatures of the second stage fluid inclusions from the Küçük Mermerlik and Karakaya locations were measured in the range of –0.8

Table 2
Representative whole-rock minor element concentrations (ppm) of the selected Kaymaz silica-listwaenite samples.

Sample	DV06	DV09	DV10	DV12	DV13	DV14	KMV14	KMV15	KMV16	KMV17	KMV18	KMV19	KKV16	KKV17	KKV18	KKV19	KKV20	KKV24	KV16	KV20	KV21	KV24	KV25	KV26
Au	9.95	18.4	9.71	13.9	34.1	14.2	0.51	2.42	13.4	15.75	2.21	6.15	4.81	78.3	7.88	2.94	4.19	2.25	4.04	2.96	5.3	9.03	12.58	23.43
Ag	9.5	18	15.1	15.1	31.8	6	2.2	1.3	8.5	8.4	3.6	2.25	9.1	34.5	10.6	4.9	2.1	1.24	4	12.2	8.2	3.51	69.25	9.21
As	2960	1310	1520	8720	10,000	1829	3210	2890	7150	7900	1855	5821	2650	2210	1330	1480	1940	3700	7130	2470	3180	840	1053	3273
Ba	1550	3430	1560	1020	50	n.a.	40	20	10	90	100	n.a.	430	270	130	160	3970	0	390	310	230	n.a.	n.a.	n.a.
Be	25.4	2.9	12.9	10.5	5.3	n.a.	0.6	<0.5	<0.5	<0.5	<0.5	n.a.	0.7	1.3	0.5	4.3	<0.5	0	6.6	4.9	4.2	n.a.	n.a.	n.a.
Cd	<0.5	<0.5	<0.5	0.5	0.7	n.a.	<0.5	<0.5	<0.5	<0.5	0.7	n.a.	<0.5	<0.5	<0.5	<0.5	17.3	n.a.	<0.5	<0.5	<0.5	<0.5	n.a.	n.a.
Co	37	15	18	39	64	n.a.	33	41	39	59	48	n.a.	29	14	47	7	7	n.a.	169	76	96	n.a.	n.a.	n.a.
Cr	3790	3050	1930	2240	2040	n.a.	2220	2310	2210	2830	1930	n.a.	2620	2690	2400	2410	81	n.a.	4440	2160	3140	n.a.	n.a.	n.a.
Ni	651	163	409	444	991	290	1345	1230	395	946	1580	1088	520	276	1315	1950	103	2950	4220	1570	1950	181	99.43	554
Bi	<2	<2	<2	4	21	n.a.	<2	<2	<2	<2	<2	0	<2	<2	3	5	<2	n.a.	3	3	<2	n.a.	n.a.	n.a.
Cu	8	15	8	8	19	11.46	10	5	17	28	27	33.14	21	11	26	17	18	28.57	77	22	26	41.13	141	66.08
Hg	1.12	0.33	0.24	0.44	1.4	n.a.	0.25	1.34	1.11	0.6	0.16	n.a.	1.29	0.831	0.62	0.15	0.81	n.a.	0.71	0.26	0.44	n.a.	n.a.	n.a.
Mn	181	150	130	112	82	99.24	307	59	55	75	211	56	82	83	305	129	32	383	2590	455	624	571	631	4343
Mo	14	4	6	10	4	n.a.	<1	1	3	<1	1	n.a.	2	6	3	6	12	n.a.	11	7	n.a.	n.a.	n.a.	n.a.
P	100	100	80	20	<10	n.a.	730	20	<10	<10	460	n.a.	140	40	500	200	360	n.a.	210	230	270	n.a.	n.a.	n.a.
Pb	88	83	45	65	156	92.65	5	2	18	16	29	202	24	57	23	48	34	34.22	58	102	72	141	57.19	157
Sb	115	52	84	90	132	n.a.	175	64	81	93	86	n.a.	30	118	24	62	19	<5	105	66	93	n.a.	n.a.	n.a.
Sc	<1	<1	<1	<1	<1	n.a.	5	5	3	4	11	n.a.	<1	<1	11	10	2	n.a.	26	13	11	n.a.	n.a.	n.a.
Sr	50	158	73	51	40	n.a.	28	14	65	115	60	n.a.	28	38	19	14	106	n.a.	60	56	51	n.a.	n.a.	n.a.
V	39	18	15	20	8	n.a.	16	32	41	35	54	n.a.	25	26	20	21	38	n.a.	112	79	63	n.a.	n.a.	n.a.
W	10	<10	<10	10	<10	n.a.	<10	<10	<10	<10	<10	n.a.	<10	<10	<10	<10	10	n.a.	10	10	10	n.a.	n.a.	n.a.
Zn	190	59	73	44	30	25.15	38	77	54	61	73	101	47	69	91	76	1305	72.81	171	112	111	1177	1415	9433
Ag/Au	0.95	0.98	1.56	1.09	0.93	0.42	4.31	0.54	0.63	0.53	1.63	0.37	1.89	0.44	1.35	1.67	0.5	0.55	0.99	4.12	1.55	0.39	5.5	0.39

*DV: Damdamca, KMV: Küçük Mermerlik, KKV: Karakaya, KV: Kızılağl, n.a: not analyzed.

to -4.1 °C and -0.8 to -2.4 °C, respectively. The salinity of the first stage fluid inclusions was calculated between 0.18 and 15.66 wt% NaCl equ. according to Bodnar and Vitky (1994), while these salinities were in the range of 1.40 – 6.63 wt% NaCl equ. in the second stage fluid inclusions for the investigated locations (Fig. 11b).

The eutectic temperatures (T_e) of some of the first stage fluid inclusions occur in some cases at positive values due to clathrate formation. Clathrate melting temperatures (T_{m-clth}) of these fluid inclusions were measured between 1.2 and 11.2 °C in all the investigated locations (Fig. 11c). The T_{m-clth} values, higher than + 10 °C, were not used for the salinity calculations; they likely reflect inclusions with significant amounts of methane and not solely H₂O and CO₂. Therefore, taking into consideration of T_{m-clth} lower than + 10 °C, the salinity of clathrate-bearing inclusions were calculated in the range of 1.24 to 14.2 wt% NaCl equ. (Table 4), according to Steele-MacInnis et al. (2012).

The relationship between T_h , salinity, and density for the Karakaya, Küçük Mermerlik, and Kızılağl mineralized zones is given in Fig. 11b. The T_h values of the first stage inclusions from these occurrences, which are characterized by clathrate formation during freezing experiments, are higher and have a wider range (Fig. 11b) when compared to those from the second stage fluid inclusion where clathrate was not observed. There are also differences in the density of the fluids forming the Kaymaz deposit. The densities of the first stage fluid inclusions, with higher T_h and salinity values, vary between 0.5 and 0.9 g/cm³, whereas the densities of the second stage fluid inclusions, having lower T_h and salinities, are close to 0.8 g/cm³ (Fig. 11b).

The T_e values of the first stage fluid inclusions in the Kızılağl ore zone vary between -49.6 and -72.1 °C (n = 9), in the Küçük Mermerlik vary between -52.6 and -57.7 °C (n = 2), and in the Karakaya ore zone vary between -47.1 and -64.5 °C (n = 10). The T_e values of the second stage fluid inclusions in the Karakaya were measured in the range of -35.8 and -54.4 °C (n = 8), while a single measurement of -48 °C was obtained from the Küçük Mermerlik mineralized zone (Table 4, Fig. 11c). Comparing these T_e values of the first stage fluid inclusions with various water-salt combinations of Shepherd et al. (1985), the T_e values close to -49.6 °C, suggest likely an H₂O-CaCl₂ dominated system. However, some values close to -56.6 °C, or lower suggest that some dissolved CO₂ and/or CH₄ may be present in these fluid inclusions even when there were no separated carbonic phases at room temperatures. Conversely, T_e values of the second stage fluid inclusions are close to compositions of H₂O-NaCl-CaCl₂, H₂O-MgCl₂-CaCl₂, and H₂O-KCl-CaCl₂ dominated system according to the T_e values between -35.8 and -54.4 °C.

5. Discussion

5.1. Geological and mineralogical features and deposit type

After the closure of the northern branch of the Neo-Tethys Ocean, the northern edge of the Anatolide-Tauride Block was metamorphosed under blueschist facies during the Late Cretaceous (Okay et al., 1996, 1998; Okay and Whitney, 2010). The collision of the Anatolide-Tauride Block and Sakarya Continent began in the Paleocene (Okay, 2011). Following the continental collision, Eocene granitoids, including the Kaymaz pluton, were widely emplaced into the greenschist facies and HP/LT blueschist facies (Harris et al., 1994; Whitney et al., 2011). The geochemical features of the Kaymaz granite resemble those of subduction-related magmas, reflecting a source region that was metasomatized by subduction-related processes (Güllü, 2012; Demirbilek, 2012; Shin et al., 2013).

The Kaymaz gold deposit, which may be related to the Eocene Kaymaz pluton, includes the Damdamca, Karakaya, and Küçük Mermerlik mineralized zones developed in serpentinites, and the Kızılağl zone hosted in quartz schists. Among these mineralized zones, Küçük Mermerlik and Kızılağl zones were formed approximately 1 km far from the Kaymaz pluton, whereas Damdamca and Karakaya ore zones were

Table 3
Representative EPMA data of the pyrite from the Kaymaz gold deposit.

Elements	Pyrite-I										Pyrite-II										
	Sampl. No	7-c2	7-c2	13-c5	13-c5	6-c5	6-c5	6-c5	15-c2	15-c2	15-c2	3	3	3	3	7	7	7	11	11	11
Analy. No	1	3	4	9	10	12	17	18	19	30	1	5	1	2	5	4	7	1	5	8	
Wt.%																					
Fe	44.25	42.87	45.86	45.39	46.07	45.62	45.45	45.84	45.88	45.86	46.07	45.88	46.00	46.26	45.48	45.70	45.75	45.65	44.11	46.12	
As	4.48	7.80	1.30	1.54	0.78	2.39	1.35	1.16	2.66	0.42	–	0.04	–	–	–	–	0.06	–	0.05	–	
Sb	–	–	–	–	–	–	–	–	0.13	–	–	–	–	–	–	–	–	–	–	–	
Ag	–	0.05	0.06	–	0.06	–	–	–	–	–	–	–	–	–	–	–	–	–	–	–	
S	51.13	48.49	52.46	52.45	53.04	52.66	52.90	52.86	50.91	53.17	53.56	53.62	53.41	53.15	53.17	53.40	53.25	53.30	52.42	53.29	
Cu	–	–	0.15	–	–	–	–	0.06	–	–	–	–	0.06	–	–	–	–	–	–	–	
Ni	0.26	–	0.32	0.11	0.13	0.13	–	–	0.15	0.35	–	0.014	–	0.11	–	–	–	0.29	0.13	–	
Co	–	–	–	–	–	–	–	–	–	–	0.57	0.40	0.37	0.38	1.64	0.67	0.98	1.95	3.49	0.63	
Se	–	0.07	–	–	–	–	–	–	–	–	–	–	–	–	–	–	–	–	–	–	
Au	0.07	0.10	–	0.05	–	0.06	0.05	–	0.05	0.06	–	–	–	–	–	–	–	–	–	–	
Hg	0.11	0.65	–	0.66	–	0.23	0.50	–	0.11	0.39	0.06	–	0.05	–	–	–	–	–	–	–	
Total	100.30	100.04	100.14	100.20	100.080	100.23	100.25	99.92	99.88	100.24	100.29	100.16	99.95	99.89	100.29	99.78	100.04	100.18	100.21	100.15	
At. Prop.																					
Fe	0.9693	0.965	0.992	0.985	0.992	0.983	0.983	0.991	1.006	0.989	0.988	0.984	0.989	0.996	0.977	0.984	0.984	0.974	0.953	0.991	
As	0.073	0.131	0.021	0.025	0.012	0.038	0.022	0.019	0.043	0.007	–	0.000	–	–	–	–	0.001	–	0.000	–	
Sb	–	–	–	–	–	–	–	–	0.001	–	–	–	–	–	–	–	–	–	–	–	
Ag	–	0.001	0.001	–	0.01	–	–	–	–	–	–	–	–	–	–	–	–	–	–	–	
S	1.951	1.902	1.977	1.983	1.989	1.977	1.992	1.990	1.945	1.997	2.000	2.004	2.001	1.994	1.990	2.002	1.995	1.981	1.972	1.995	
Cu	–	–	0.003	–	–	–	–	0.001	–	–	–	–	0.001	–	–	–	–	–	–	–	
Ni	0.001	–	0.007	0.002	0.003	0.003	–	–	0.003	0.007	–	0.003	–	0.001	–	–	–	0.006	0.003	–	
Co	–	–	–	–	–	–	–	–	–	–	0.12	0.008	0.008	0.008	0.033	0.014	0.020	0.039	0.071	0.013	
Se	–	0.001	–	–	–	–	–	–	–	–	–	–	–	–	–	–	–	–	–	–	
Au	0.001	0.001	–	0.000	–	0.001	0.000	–	0.000	0.001	–	–	–	–	–	–	–	–	–	–	
Hg	0.001	0.003	–	0.03	–	0.001	0.003	–	0.001	0.002	0.000	–	0.000	–	–	–	–	–	–	–	
Total	3	3	3	3	3	3	3	3	3	3	3	3	3	3	3	3	3	3	3	3	

* - below detection limit.

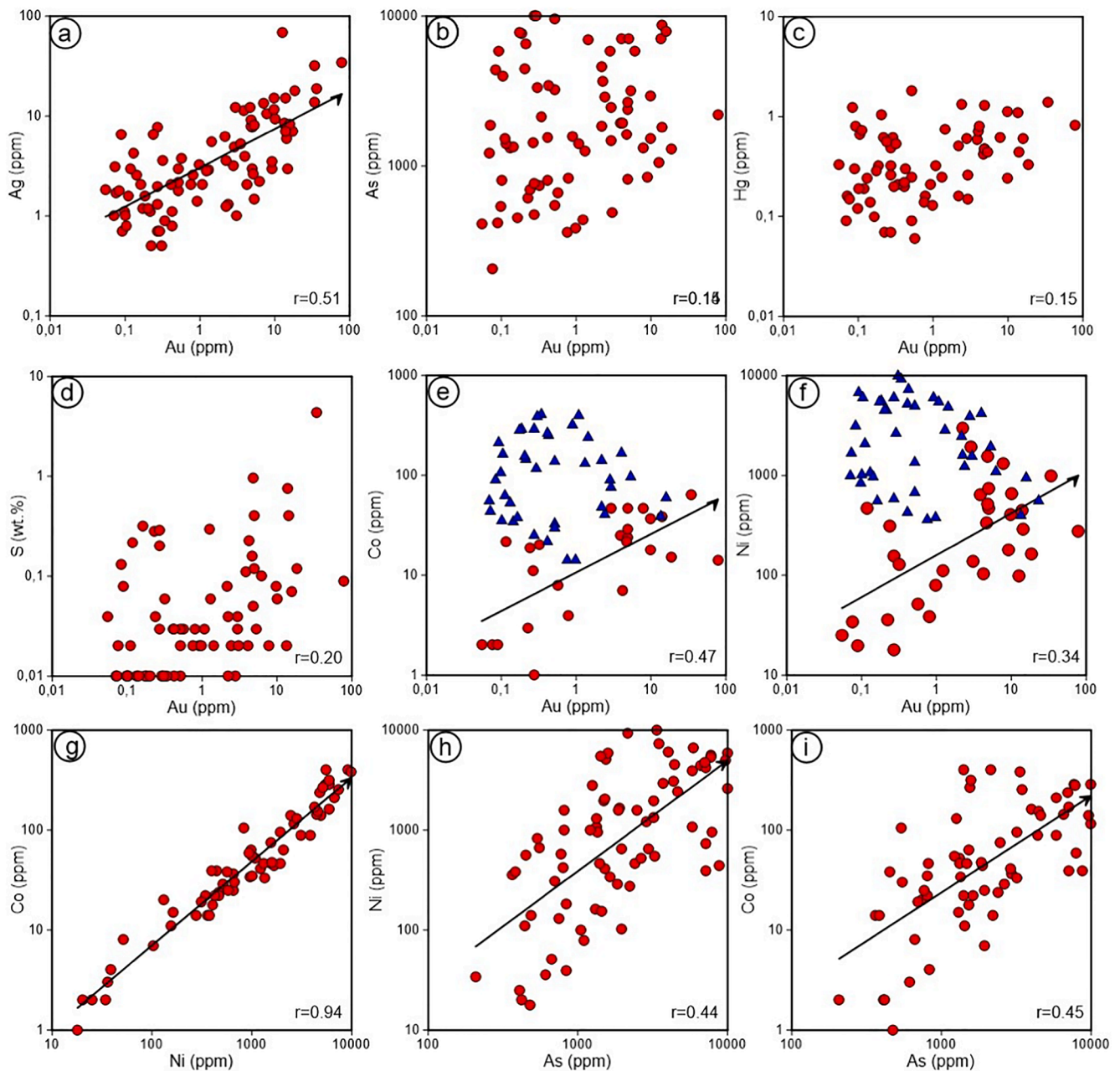


Fig. 9. Correlative relations among Au, As, Ag, Hg, S, Co, and Ni elements measured from the whole-rock samples of the Kaymaz listwaenite (triangle symbols in Figures d and e represent the whole-rock samples of the Kızılağul and Küçük Mermerlik mineralizations).

formed close to the Kaymaz pluton (Fig. 3). There are no significant differences between these ore veins in terms of both the host rock and their relationship with the granitoid. Similar textural features such as vuggy, cockade, and comb were described in all of them, which refer to low to medium temperature conditions. Similar mineral paragenesis has also been defined in these veins. According to this, in the veins where two different ore stages were defined, the first stage is characterized by pyrite-I, arsenopyrite, marcasite, nickeline, pentlandite, millerite, and bravoite minerals, and gold and silver accompany this stage, while the second stage is characterized by pyrite-II and minor chalcopyrite (Fig. 7). The ore minerals in the Damdamca, Karakaya, and Küçük Mermerlik zones show similarity with the silica-carbonate classification of Tüysüz and Eler (1993), taking into consideration of ore and host-rock relation, carbonate-silica alteration, and supergene overprinting.

5.2. Formation conditions and boiling evidence from fluid inclusions

Two different ore stages were further confirmed for the Kaymaz gold deposit by the fluid inclusion results. According to these results, T_h of the first stage hydrothermal fluids is between 282 and 389 °C, while these temperatures are in the range of 237–298 °C for the second stage (Fig. 11a). The salinity values of these fluid inclusions are also significantly different. Accordingly, the salinity of the first stage hydrothermal fluids are in the range of 0.18 and 15.65 wt% NaCl equ. while the salinity of the second stage hydrothermal fluids ranges from 0.8 to 6.64 wt% NaCl equ. The T_h -salinity range of the first stage fluid inclusions in Fig. 11b shows well appropriate distribution with the isothermal mixing trend, which indicates a mixture of two different solutions. Although the temperature values remain constant in this trend, the salinity decreases down to 0 wt% NaCl equ. which indicates the mixture of two different solutions with high and low salinity.

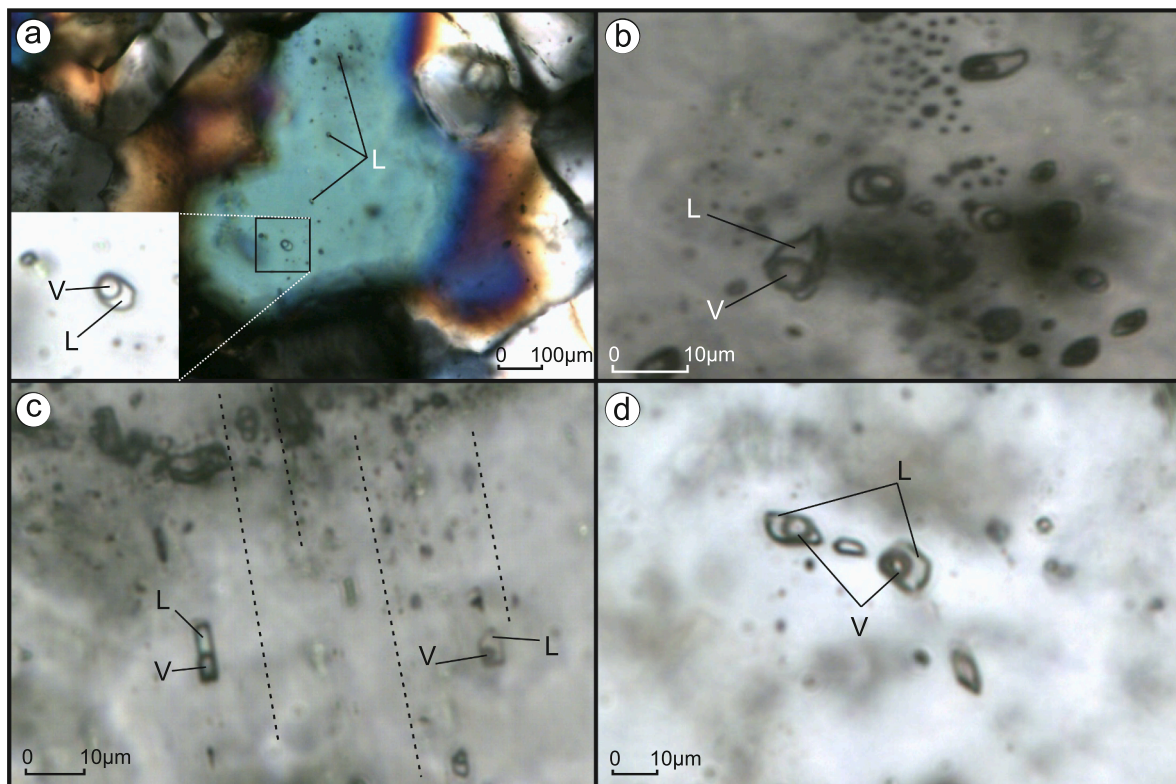


Fig. 10. a) Two-phase, liquid-rich fluid inclusions observed in jigsaw quartz minerals, b) Coexistence of vapor-rich and liquid-rich fluid inclusion in the first stage quartz, c) Tube-shaped fluid inclusions and their rephrase along the growth zones, d) Coexistence of vapor- and liquid-rich fluid inclusion in the first stage quartz.

Table 4

Summary of microthermometric data of fluid inclusions obtained from the gold-bearing quartz veins of the Kaymaz gold deposit.

Location	Stage	Type	Mode	Statistic Param.	Te, (°C)	Tm-ice (°C)	Tm-clth (°C)	Salinity (Wt.%)	Th, (°C)
Küçük Mermerlik	Stage-I	Type-I	Liquid	Max	-57.7	-	3	14.2	389
				Min	-52.6	-	1.2	11.9	282
				n	2	-	2	2	19
	Type-II	Vapor	Max	-	-7.3	-	11	370	
			Min	-	-0.6	-	1.1	298	
			n	-	3	-	3	3	
Stage-II	Type-I	Liquid	Max	-48	-0.8	-	6.6	268	
			Min	-48	-4.1	-	1.4	238	
			n	1	7	-	7	7	
Kızılağul	Stage-I	Type-I	Liquid	Max	-64.6	-1.5	9.1	7.5	382
				Min	-49.6	-0.1	6	0.2	285
				n	6	9	6	15	18
	Type-II	Vapor	Max	-64.2	-	10	9.8	364	
			Min	-56.8	-	4.5	0	279	
			n	3	-	7	7	7	
Karakaya	Stage-I	Type-I	Liquid	Max	-64.5	-8.9	7.7	12.9	374
				Min	-47.1	-0.4	4.8	0.7	316
				n	10	16	4	20	25
	Type-II	Vapor	Max	-63.6	-11.4	8.3	15.7	372	
			Min	-47.4	-2.4	5.6	3.4	327	
			n	5	3	3	6	6	
Stage-II	Type-I	Liquid	Max	-54.4	-2.4	-	4.0	298	
			Min	-35.8	-0.8	-	1.4	237	
			n	8	23	-	23	25	

The authors declare that they have no known competing financial interests or personal relationships that could have appeared to influence the work reported in this paper.

The coexistence of liquid- and vapor-rich fluid inclusions with rather similar homogenization temperature range confirm that there was boiling in the Kaymaz gold deposit. Besides, observation of jigsaw, colloform, and polymose ore textures, which are characteristically reported from epithermal ore deposits, are evidence of boiling (Moncada

et al., 2012). Therefore, it is suggested that metals may have been precipitated along the fault zones during the boiling event in the Kaymaz silica-listwaenites. In this scenario, Kaymaz granite is the possible source for the formation of the gold deposit that possibly provided a heat source for the fluids.

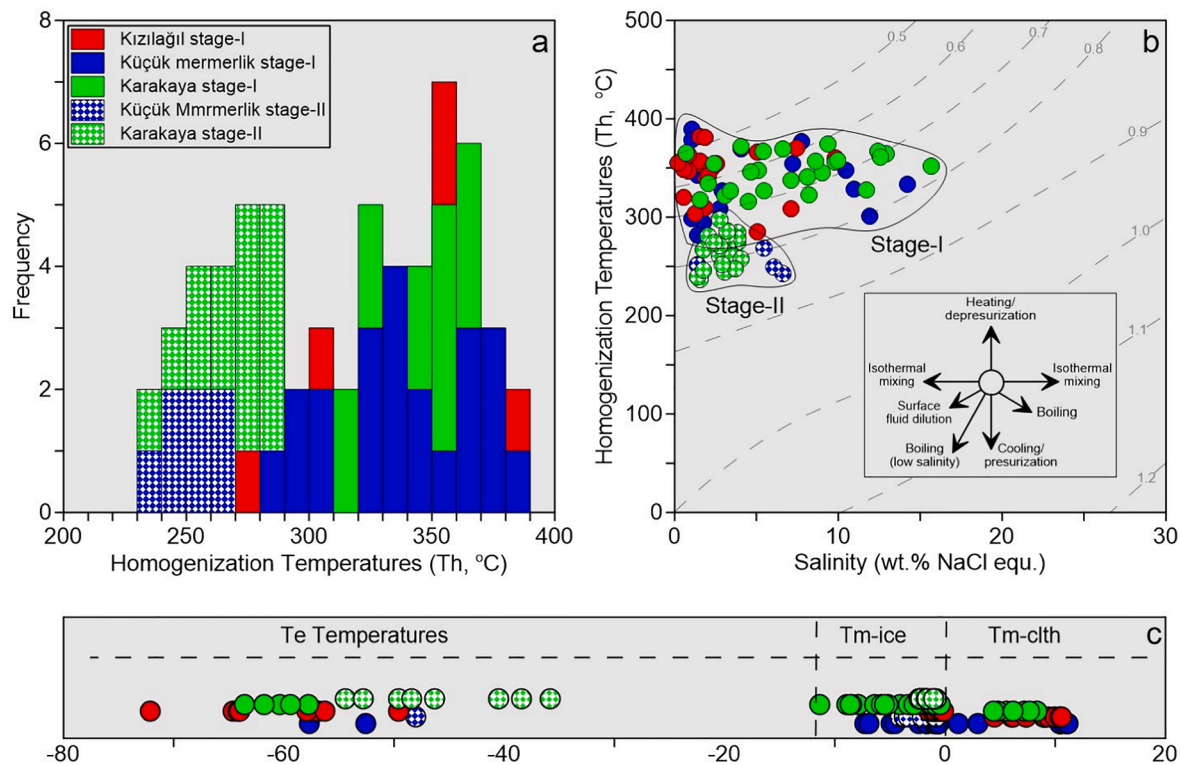


Fig. 11. a) Homogenization temperature frequency histograms of the first and second stage fluid inclusions from the Kaymaz listwaenite, b) T_h -salinity relations of both stage fluid inclusions and comparison with the typical T_h -salinity trends of various fluid evolution processes (Wilkinson, 2001), c) T_e , T_{m-ice} and T_{m-clth} ranges of both stage fluid inclusions.

During the freezing/melting experiments, CO_2 bearing vapor phase was not observed. However, the average of the T_e values (-57.9°C) of first stage inclusions in the jigsaw quartz is very close to the T_e value of pure CO_2 (-56.6°C), indicating that the fluids may contain CO_2 . In some inclusions, T_{m-clth} values are higher than $+10^\circ\text{C}$, indicating that the inclusions contain not only CO_2 but also other non-aqueous gases such as CH_4 (van den Kerkhof and Theiry, 2001; Wilkinson, 2001; Zoheir and Lehmann, 2011; Aliyari et al., 2020). In light of these data, the hydrothermal fluids are best defined by the $\text{H}_2\text{O} + \text{NaCl} + \text{CO}_2 \pm \text{CH}_4$ system. The possible source of the CO_2 and CH_4 is probably the ultramafic host rocks because it is known that ultramafic rocks can produce inorganic carbon (Welhan, 1988). Thus, these carbon-bearing gases in the fluid inclusions show that the ore-forming fluid interacted significantly with the ultramafic host rocks.

5.3. Source and evolution of hydrothermal fluids

According to whole-rock geochemical analysis, the Kaymaz silica-listwaenites are characterized by high Ni (up to 9950 ppm), Fe (up to 18.8 wt%), and Cr (>10 wt%) contents, while Co (up to 408 ppm) was relatively lower in these samples. In addition to the higher Ni, Fe and Cr contents, positive correlations between Ni-Co and Fe-Cr, as well as Ni/Co ratios close to 21, were considered as evidence of mafic-ultramafic source rocks for these elements in some studies (Blevin and Chappell, 1992; Ho et al., 1995; Demir and Bayraktar, 2020).

According to the trace element analyses of the whole-rock samples, there is a strong positive correlation between Au and Ag in each mineralized zone (Fig. 9a), but the correlation of Au versus As, Hg, and S is weak (Fig. 9b, c, d). Gold in these zones has no association with base metals such as Pb, Zn, and Cu and also has limited correlative relations with Co and Ni in the mineralized zones (Fig. 9e, f). Moreover, there is a limited relationship between As and these elements (Fig. 9h, i). However, in the mineral chemistry analyses, Au and As content of the pyrite-I are as much as 0.1 wt% and 7.8 wt%, respectively. Gold in these pyrites

always correlated with As (Fig. 8c). Therefore, high As content and positive correlation between As and Au in pyrite-I reflect features of the first stage hydrothermal solution, which indicate that As and Au were not derived from the same source as Ni, Co, and Cr.

The close association between Au and As in pyrite-I suggests that these metals were in equilibrium in hydrothermal solutions. Conversely, the negative correlation of Au with Ni and Co demonstrates that Ni and Co were locally derived from the ultramafic host rocks into the ore-forming fluids. According to Likhoidov et al. (2007), the weak association between Au, and Ni and Co may indicate that the hydrothermal fluids did not carry these elements at the same time during the formation of listwaenites. Alternatively, the Ni, Co, and Au complexes were not in equilibrium with each other in the hydrothermal solutions during their transportation. Similar findings were also reported by Uçurum (1998) and Li et al. (2018) that As was not equilibrated with Ni and Co in hydrothermal fluids. In various studies, it has been pointed out that gold enrichment in listwaenites is related to the introduction of silica phases, related to granitic intrusion (Buisson and Leblanc, 1985; Uçurum, 2000; Akbulut et al., 2006). According to these studies, the association of Au with other metallic minerals in the silica phase is not common. Taking into consideration of all these explanations, it is suggested that an increased content of As and Au in listwaenites were likely of a magmatic-hydrothermal origin, while the presence of elevated Cr, Ni, and Co demonstrates the contribution from an ultramafic host rock by the interaction of hydrothermal fluids. The magmatic origin of the first stage hydrothermal solutions is in agreement with the sulfur isotope data (-4.7 and 2.6%) reported by Toygar (2014).

Two different stages of pyrite formation have been recognized by the ore microscopy study, and gold and silver were observed to have always been accompanied by the pyrite-I. These first-stage pyrite grains are characterized by higher Ni content (generally between 0.1 and 0.8 wt%; in a single grain 9.1 wt%) and contain minor Au and As. On the contrary, second stage pyrite is characterized by higher Co and Au, and As contents of these pyrite grains are always lower than the detection limits.

Taking into consideration of the high Ni content of ultramafic host rocks, the higher Ni contents of the pyrite-I confirm that the ore forming fluids interacted with ultramafic host rocks. However, distinctly higher Co and lower Ni content of the pyrite-II point to different sources.

The higher Co content of the pyrite-II was also arguably accepted as the source of basic-ultrabasic sources in the pioneering studies (Raymond, 1996; Demir et al., 2015; Zhao et al., 2011; Wang et al., 2018). Therefore, while the gold-bearing pyrite-I in the Kaymaz listwaenites is associated with ultramafic host rocks, the higher Co content of the second stage gold-free pyrite should likewise be associated with another ultramafic source. In the Kaymaz area, both sedimentary units and the Kaymaz granite have no potential to produce high Co. In this case, the only possible source of second stage pyrite, with higher Co contents, maybe metabasites of the Halilbağı Formation. The lower T_h and salinity values of the second stage fluid inclusions, and their CO_2 and CH_4 free compositions, as well as the lower As and Au contents of the second stage pyrite, supports the idea that second stage ore is not related to serpentinites, but derived from another basic unit of metabasites by the circulation of the meteoric dominated hydrothermal fluids. The contribution of meteoric solutions in the second stage of the Kaymaz gold deposit is also compatible with the oxygen isotope data (between 21.5 and 31.7‰) reported by Toygar (2014) from quartz minerals.

6. Conclusions

The Kaymaz gold deposit includes four mineralized zones: Damdamca, Karakaya, and Küçük Mermerlik hosted in the serpentinites, and Kızılağıl located in quartz schist. The Damdamca and Karakaya mineralized zones were formed in close proximity to the Kaymaz pluton, while the Küçük Mermerlik and Kızılağıl ore zones were located ~1 km distance on the surface. Structural, mineralogical, and lithological features, including the formation of low- to moderate-temperature vuggy, cockade, and comb quartz textures, indicate that similar systems were effective in controlling all these mineralized zones.

Microscopic studies indicate that sulfide minerals such as pyrite-I, arsenopyrite, marcasite, nickeline, pentlandite, millerite, and bravoite were formed at the beginning of the first hydrothermal stage, while native gold and silver grains were formed through the end of this stage. Pyrite-II and limited chalcopyrite were also defined at the second hydrothermal stage. However, no genetic relationship was defined between the native Au-Ag and the second stage sulfides.

Whole-rock samples of the listwaenites are rich in Ni, Cr, and Co, and their Ni/Co ratios (~21) are similar to that of the ultramafic rocks, signifying contributions of these elements from the local country rock. However, a distinct lack of correlations between As and/or Au with the Ni and/or Co concentrations indicates that As and Au originated from the intrusion of the Kaymaz pluton.

According to mineral chemistry analysis, the pyrite-I was found to be enriched in As and Au. However, both As and Au concentrations of the pyrite-II are always lower than detection limits, and Co concentrations of these pyrite-II are higher than the pyrite-I. Therefore, the interaction between hydrothermal fluids and another basic unit belonging to the Halilbağı Formation was suggested for the second stage of hydrothermal fluids.

The coexistence of fluid- and vapor-rich fluid inclusions with similar T_h and salinity values indicate that gold and silver precipitation in the Kaymaz gold deposit resulted by boiling of hydrothermal fluids.

Due to the fact that T_e values of the first stage fluid inclusions are close to melting temperatures of CO_2 and clathrate formation detected in some fluid inclusions, it can be confirmed that hydrothermal fluids included carbonic phases such as CO_2 and CH_4 .

These carbonic phases also suggest that hydrothermal fluids have interacted significantly with ultramafic host rocks at the first stage. However, in addition to lower T_h and salinity values, the distinct lack of CO_2 and CH_4 phases at the second stage fluid inclusions are consistent with the idea that gold and silver-free meteoric fluids interacted with the

metabasites instead of the serpentines.

CRediT authorship contribution statement

Hikmet Yavuz: Conceptualization, Methodology, Investigation, Resources, Writing – original draft, Validation. **Yılmaz Demir:** Conceptualization, Methodology, Investigation, Software, Data curation, Formal analysis, Validation, Writing – original draft, Writing – review & editing. **Cem Kasapçı:** Investigation, Data curation, Validation, Resources, Writing – original draft, Writing – review & editing. **İbrahim Uysal:** Data curation, Formal analysis, Visualization, Validation, Writing – review & editing. **Cahit Helvacı:** Supervision, Project administration, Conceptualization, Methodology, Investigation, Data curation, Visualization, Writing – review & editing.

Declaration of Competing Interest

The authors declare that they have no known competing financial interests or personal relationships that could have appeared to influence the work reported in this paper.

Acknowledgment

Koza Gold Corporation supported this work. The authors express their gratitude to Richard J. Goldfarb for his helpful comments and critical reading of an early version of the manuscript. We also wish to thank Nurullah Hanilçı for assistance with the fluid inclusion studies and their interpretation. Two anonymous reviewers are thanked for their perceptive comments during the revision of the manuscript. Thanks are also due to Emrah Yalçın Ersoy for his comments on regional geology.

References

- Akbulut, M., Pişkin, Ö., Karayığit, A.H., 2006. The genesis of the carbonatized and silicified ultramafics known as listwaenites: a case study from the Mihalıççık region (Eskişehir), Northwest Turkey. *Geol. J.* 41, 557–580.
- Aliyari, F., Demir, Y., Bouzari, F., 2020. Geology, geochemistry, fluid inclusions and genesis of the Gujeh Qaleh IOA-type iron deposit, North of Takab district, Northwestern, Iran. *Ore Geol. Rev.* 127, 103835.
- Altunkaynak, S., Dilek, Y., Genç, S.C., Sunal, G., Gertisser, R., Furnes, H., Foland, K.A., Yang, J., 2012. Spatial, temporal and geochemical evolution of Oligo-Miocene granitoid magmatism in western Anatolia, Turkey. *Gondwana Res.* 21, 961–986.
- Auclair, M., Gauthier, M., Trottier, J., Jébrak, M., Chartrand, F., 1993. Mineralogy, geochemistry, and paragenesis of the Eastern Metals serpentinite-associated Ni-Cu-Zn deposit, Quebec Appalachians. *Economic Geology*, 88, 123–138.
- Aydal, D., 1989. Gold-bearing listwaenites in the Arac, Massif, Kastamonu, Turkey. *Terra Nova* 2, 43–52.
- Blevin, P.L., Chappell, B.W., 1992. The role of magma sources, oxidation states and fractionation in determining the granite metallogeny of eastern Australia. *Transactions of the Royal Society of Edinburgh, Earth Science* 83, 305–316.
- Bodnar, R.J., Vitky, M.O., 1994. Interpretation of microthermometric data for H₂O-NaCl fluid inclusions. In *Fluid inclusions in minerals, Method and Appl.* (ed. B.De Vivo and M.L. Frezotti), Virginia Tech. 117–130.
- Buckman, S., Ashley, P., 2010. Silica-carbonate (listwaenites) related gold mineralisation associated with epithermal alteration of serpentinite bodies. <https://ro.uow.edu.au/scipapers/715>.
- Buisson, G., Leblanc, M., 1985. Gold in carbonatized ultramafic rocks from ophiolite complexes. *Econ. Geol.* 80, 2026–2029.
- Buisson, G., Leblanc, M., 1986. Gold-bearing listwaenites (carbonatized ultramafic rocks) from ophiolite complexes. In: Gallagher, J.M., Ixer, R.A., Neary, C.R. (Eds.), *Metallogeny of Basic and Ultrabasic Rocks*. Institution of Mining and Metallurgy, London, pp. 121–132.
- Buisson, G., Leblanc, M., 1987. Gold in mantle peridotites from Upper Proterozoic ophiolites in Arabia, Mali, and Morocco. *Econ. Geol.* 82, 2091–2097.
- Çiftçi, Y., 2001. Kızıldağ (Refahiye-Erzincan) lisfenitlerinin jeolojisi mineralojisi ve Au-PGE jeokimyası. *Istanbul University, The Faculty of Engineering Earth Science Magazine* 2, 27–49.
- Darling, S.R., 1991. An extended equation to calculate NaCl contents from final clathrate melting temperatures in H₂O-CO₂-NaCl fluid inclusions: Implications for P-T isochore location. *Geochim. Cosmochim. Acta* 55, 3869–3871.
- Demir, Y., Uysal, I., Sadıklar, M.B., Ceriani, A., Hanilçı, N., Müller, D., 2015. Mineralogy, mineral chemistry, fluid inclusion, and stable isotope investigations of the Kabadüz ore veins, Ordu, NE-Turkey. *Ore Geology Reviews*, 66, 82–98.
- Demir, Y., Bayraktar, K., 2020. Geochemistry, microthermometry, and C and O isotope constraints on the origin of the Düzköy Fe-Cu skarn deposit (Gümüşhane, NE Turkey). *Arab. J. Geosci.* 13 (23), 1–27.

- Demirbilek, M., 2012. Günyüzü, Sivrihisar ve Kaymaz bölgelerindeki (Eskişehir) sokulum kayaçlarının oluşumuna yönelik jeokimyasal, jeokronolojik ve izotopik bulgular, PhD Thesis, Eskişehir Osmangazi University, Engineering Faculty, 375 pp (unpublished).
- Gautier, Y., 1984. Déformations et métamorphismes associés à la fermeture téthysienne en Anatolie centrale (région de Sivrihisar, Turquie). PhD thesis, University Paris-Sud, France, 236.
- Göncüoğlu, M.C., Yalınz, M.K., Tekin, U.K., 2006. Geochemistry, tectono-magmatic discrimination and radiolarian ages of basic extrusives within the Izmir-Ankara suture belt (NW Turkey); time constraints for the Neotethyan evolution. *Ofioliti* 31, 25–38.
- Güllü, B., 2012. Yüksek Lisans Topkaya ve Karakaya (Eskişehir) Granitoidlerinin Zamansal ve Mekansal Konumları, MsC Thesis, University of Ankara, Ankara, (Unpublished).
- Halls, C., Zhao, R., 1995. Listvenite and related rocks: perspectives on terminology and mineralogy with reference to an occurrence at Cregganbaun, Co., Mayo. Republic of Ireland. *Mineralium Deposita* 30, 303–313.
- Harris, N.B.W., Kelley, S., Okay, A.I., 1994. Post-collision magmatism and tectonics in northwest Anatolia. *Contrib. Miner. Petrol.* 117 (3), 241–252.
- Ho, S.E., McQueen, K.G., McNaughton, N.J., Groves, D.I., 1995. Lead isotope systematics and pyrite trace element geochemistry of two granitoid associated mesothermal gold deposits in the southern Lachlan fold belt. *Economic Geology* 90, 1818–1830.
- Kashkai, M.A., Allakhverdiev, S.H.I., 1965. Listvenites, their origin and classification. *Institute Geologim. Akad. I.M. Gubkina; Izdat. Akad. Nauk Azerbaidzhanskoi SSR, Baku*, 142 pp (in Russian).
- Kaya, O., 1972. Tavşanlı yöresi ofiyolit sorununun ana çizgileri. *Türkiye Jeoloji Kurumu Bülteni* 15, 26–108.
- Korobeynikov, A.F., Goncharenko, A.I., 1986. Gold in ophiolite complexes in the Altai-Sayan folded region. *Geochimica* 1, 49–62.
- Leblanc, M., Fischer, W., 1990. Gold and platinum group elements in cobalt-arsenide ores: hydrothermal concentration from a serpentinite source-rock (Bou Azzer, Morocco). *Mineral. Petrol.* 42, 197–209.
- Leblanc, M., Lbouabi, M., 1988. Native silver mineralization along a rodingite tectonic contact between serpentinite and quartz diorite (Bou Azzer, Morocco). *Econ. Geol.* 83, 1379–1391.
- Li, N., Deng, J., Yang, L., Groves, D.I., Liu, X.W., Dai, W.G., 2018. Constraints on depositional conditions and ore-fluid source for orogenic gold districts in the West Qinling Orogen, China: Implications from sulfide assemblages and their trace-element geochemistry. *Ore Geol. Rev.* 102, 204–219.
- Likhoidov, G.G., Plyusnina, L.P., Shcheka, Z.A., 2007. The behavior of gold during listvenitization; experimental and theoretical simulation. *Dokl. Earth Sci.* 415, 723–726.
- Moncada, D., Mutchler, S., Nieto, A., Reynolds, T.J., Rimstidt, J.D., Bodnar, R.J., 2012. Mineral textures and fluid inclusion petrography of the epithermal Ag–Au deposits at Guanajuato, Mexico: Application to exploration. *J. Geochem. Explor.* 114, 20–35.
- Mta, 2002. Geological map of Turkey: Istanbul and Izmir sheets, scale 1:500,000. MTA Publication, Ankara.
- Nikiforov, A.V., Öztürk, H., Altuncu, S., Lebedev, V.A., 2014. Kızılcaören Ore-bearing Complex with Carbonatites (Northwestern Anatolia, Turkey): Formation Time and Mineralogy of Rocks. *Geol. Ore Deposits* 56 (1), 35–60.
- Okay, A.I., 1986. High pressure/low-temperature metamorphic rocks of Turkey. *Geol. Soc. Am. Mem.* 164, 333–348.
- Okay, A.I., 2011. Tavşanlı Zone: The northern subducted margin of the Anatolide-Tauride Block. *Bulletin of the Mineral Research and Exploration* 142, 191–221.
- Okay, A.I., Kelley, S.P., 1994. Tectonic setting, petrology and geochronology of jadeite+glaucophane and chloritoid+glaucophane schists from northwest Turkey. *J. Metamorph. Geol.* 12, 455–466.
- Okay, A.I., Satır, M., Maluski, H., Siyako, M., Monie, P., Metzger, R., 1996. Paleo- and Neo-Tethyan events in northwest Turkey: Geological and geochronological constraints. *The Tectonic Evolution of Asia* 19, 420–441.
- Okay, A.I., Harris, N.B.W., Kelley, S.P., 1998. Exhumation of blueschists along a Tethyan suture in northwest Turkey. *Tectonophysics* 285, 275–299.
- Okay, A.I., Tüysüz, O., 1999. Tethyan sutures of northern Turkey. *Geological Society of London* 156, 475–515.
- Okay, A.I., Satır, M., Shang, C.K., 2008. Ordovician metagranitoid from the Anatolide-Tauride Block, northwest Turkey -geodynamic implications. *Terra Nova* 20, 280–288.
- Okay, A.I., Whitney, D.L., 2010. Blueschists, Eclogites, Ophiolites and Suture Zones In Northwest Turkey: A Review And A Field Excursion Guide. *Ofioliti* 35 (2), 131–172.
- Robertson, A.H.F., Ustaömer, T., 2009. Upper Palaeozoic Subduction/Acretion Processes In The Closure Of Palaeotethys: Evidence From The ChiosMelange (E Greece), The Karaburun Melange (W Turkey), and the Teke Dere Unit (SW Turkey). *Sed. Geol.* 220, 29–59.
- Roedder, E., 1984. Fluid Inclusions. *Mineralogical Society of America*, Washington.
- Saraç, G., 2003. Türkiye Omurgalı Fosil Yatakları (Vertebrate Fossil Beds of Turkey). Mineral Research and Exploration Institute (MTA) of Turkey Report, Ankara, Turkey (in Turkish, Unpublished).
- Sarıfakıoğlu, E., Özen, H., Hall, C., 2009. Petrogenesis of extension-related alkaline volcanism in Karaburhan, (Sivrihisar–Eskişehir), NW Anatolia, Turkey. *J. Asian Earth Sci.* 35, 502–515.
- Seaton, N.C.A., Whitney, D.L., Teyssier, C., Toraman, E., Heizler, M.T., 2009. Recrystallization of high-pressure marble (Sivrihisar, Turkey). *Tectonophysics* 479, 241–253.
- Selçuk, A.S., Gökten, Y.E., 2012. Neotectonic Characteristics of the İnönü-Eskişehir Fault System in the Kaymaz (Eskişehir) Region: Influence on the Development of the Mahmudiye-Çift eler-Emirdağ Basin. *Turkish Journal Earth Sciences* 21, 521–545.
- Shepherd, T.J., Rankin, A.H., Alderton, D.H.M., 1985. A practical guide to fluid inclusion studies. Blackie, California.
- Sherlock, R.L., Logan, M.A.V., 1995. Silica-carbonate alteration of serpentinite, implications for the association of mercury and gold mineralization in northern California. *Explor. Min. Geol.* 4, 395–409.
- Sherlock, S., Kelley, S.P., Inger, S., Harris, N., Okay, A.I., 1999. 40Ar-39Ar and Rb-Sr geochronology of high-pressure metamorphism and exhumation history of the Tavşanlı Zone, NW Turkey. *Contrib. Miner. Petrol.* 137, 46–58.
- Shin, A.T., Catlos, J.E., Jacob, L., Black, K., 2013. Relationships between very high-pressure subduction complex assemblages and intrusive granitoids in the Tavşanlı Zone, Sivrihisar Massif, central Anatolia. *Tectonophysics* 595–596, 183–197.
- Steele-MacInnis, M., Lecumberri-Sanchez, P., Bodnar, R.J., 2012. HOKIEFLINCS H2O-NACL: A Microsoft Excel spreadsheet for interpreting microthermometric data from fluid inclusions based on the PVTX properties of H₂O–NaCl. *Comput. Geosci.* 49, 334–337.
- Şahin, Y., Örgün, Y., Güngör, Y., 2006. U/Th Ca Zengin Radioaktif Granitoidlerin Jeokimyası: Kestanbol Ve Kaymaz Plütonları, Batı Anadolu, Türkiye, Bildir Özleri, Ankara., 59. Türkiye Jeoloji Kurultayı, Ankara, 20-24 Mart, pp 43–44.
- Tekin, U.K., Göncüoğlu, M.C., Turhan, N., 2002. First evidence of Late Carnian radiolarians from the Izmir-Ankara suture complex, central Sakarya, Turkey: Implications for the opening age of the Izmir-Ankara branch of Neo-Tethys. *Geobios* 35, 127–135.
- Toygaz, Ö., 2014. Kaymaz (Eskişehir) Altın Yatağının Oluşumu Üzerine Jeokimyasal ve İzotopik Sınırlamalar. MsC Thesis, Eskişehir Osmangazi University, FBE, 131 pp (unpublished).
- Tüysüz, N., Erlar, A., 1993. Geochemistry and evolution of listwaenites in the Kağızman region (Kars, NE-Turkey). *Chem. Erde* 53, 315–329.
- Uçurum, A., 1996. Geology, geochemistry and mineralization of the silica carbonate alteration (listwaenite) from Late Cretaceous ophiolitic melanges at Cüreik-Divriği in Sivas Province and at Güvenç, Karakuz-Hekimhan in Malatya Province, Central East Turkey. Doctor of Philosophy Thesis, University of Nevada, Reno, USA.
- Uçurum, A., 1998. Application of the correspondence-Type geostatistical analysis on the Co, Ni, As, Ag and Au concentrations of the listwaenites from serpentinites in the Divriği and Kuluncak Ophiolitic Melanges. *Turkish Journal of Earth Science* 7, 87–95.
- Uçurum, A., 2000. Listwaenites in Turkey: Perspectives on formation and precious metal concentration with reference to occurrences in East-Central Anatolia. *Ofioliti* 25, 15–29.
- Van den Kerkhof, A.M., Hein, U.F., 2001. Fluid inclusion petrography. *Lithos* 55, 27–47.
- Van den Kerkhof, A.M., Theiry, R., 2001. Carbonic inclusions. *Lithos* 55, 49–68.
- Welhan, J.A., 1988. Origin of methane in hydrothermal systems. *Chem. Geol.* 71, 183–198.
- Whitney, D., Teyssier, C., Toraman, E., Seaton, N., Fayon, A., 2011. Metamorphic and tectonic evolution of a structurally continuous blueschist-to-Barrovian terrane, Sivrihisar Massif, Turkey. *J. Metamorph. Geol.* 29, 193–212.
- Wilkinson, J.J., 2001. Fluid inclusions in hydrothermal ore deposits. *Lithos* 55, 229–272.
- Yavuz, H., 2013. Kaymaz (Eskişehir) Listvenitik Altın Yatağı'nın Özellikleri ve Kökenine Bir Yaklaşım. MsC Thesis, University of Dokuz Eylül, FBE, İzmir, Turkey.
- Yavuz, H., Helvacı, C., Demir, Y., Kasapçı, C., Uysal, I., 2013. Preliminary findings on the mineralogical and fluid inclusion properties of Kaymaz (Eskişehir) Gold Deposit, Turkey. *Abstract of European Current Research On Fluid Inclusions* 22, 109–111.
- Yiğit, Ö., 2006. Gold in Turkey- a missing link in Tethyan metallogeny. *Ore Geol. Rev.* 28, 147–179.
- Yiğit, Ö., 2009. Mineral deposits of Turkey in relation to Tethyan metallogeny: implications for future mineral exploration. *Econ. Geol.* 104, 19–51.
- Yiğit, Ö., 2012. Discovered and undiscovered gold endowment of Turkey: a quantitative mineral resource assessment using GIS and rank statistical analysis. *Miner. Deposita* 47, 521–534.
- Zhelobov, P., 1979. Alpine type hyperbasite rocks as a probable source of gold. *Int. Geol. Rev.* 23, 347–353.
- Zoheir, B., Lehmann, B., 2011. Listvenite lode association at the Barramiye gold mine, Eastern Desert. *Egypt. Ore Geology Reviews* 39, 101–115.